frontiers | Frontiers in Cellular Neuroscience

ORIGINAL RESEARCH
published: 30 June 2022
doi: 10.3389/fncel.2022.912030

Neuronal Adenosine A_1 Receptor Is Critical for Olfactory Function but Unable to Attenuate Olfactory Dysfunction in Neuroinflammation

Charlotte Schubert[1], Kristina Schulz[2], Simone Träger[1], Anna-Lena Plath[3], Asina Omriouate[3], Sina C. Rosenkranz[1], Fabio Morellini[3], Manuel A. Friese[1†] and Daniela Hirnet[2*†]*

[1] Institute of Neuroimmunology and Multiple Sclerosis (INIMS), University Medical Center Hamburg-Eppendorf, Hamburg, Germany, [2] Division of Neurophysiology, Institute of Cell and Systems Biology of Animals, University of Hamburg, Hamburg, Germany, [3] Research Group Behavioral Biology, Center for Molecular Neurobiology (ZMNH), University Medical Center Hamburg-Eppendorf, Hamburg, Germany

OPEN ACCESS

Edited by:
Carl Edward Schoonover, Columbia University, United States

Reviewed by:
Peter Illes, Leipzig University, Germany
Nicola Kuczewski, Université Claude Bernard Lyon 1, France

***Correspondence:**
Manuel A. Friese
manuel.friese@zmnh.uni-hamburg.de
Daniela Hirnet
daniela.hirnet@uni-hamburg.de

† These authors have contributed equally to this work

Specialty section:
This article was submitted to Cellular Neurophysiology, a section of the journal Frontiers in Cellular Neuroscience

Received: 03 April 2022
Accepted: 08 June 2022
Published: 30 June 2022

Citation:
Schubert C, Schulz K, Träger S, Plath A-L, Omriouate A, Rosenkranz SC, Morellini F, Friese MA and Hirnet D (2022) Neuronal Adenosine A_1 Receptor Is Critical for Olfactory Function but Unable to Attenuate Olfactory Dysfunction in Neuroinflammation. Front. Cell. Neurosci. 16:912030. doi: 10.3389/fncel.2022.912030

Adenine nucleotides, such as adenosine triphosphate (ATP), adenosine diphosphate (ADP), as well as the nucleoside adenosine are important modulators of neuronal function by engaging P1 and P2 purinergic receptors. In mitral cells, signaling of the G protein-coupled P1 receptor adenosine 1 receptor (A_1R) affects the olfactory sensory pathway by regulating high voltage-activated calcium channels and two-pore domain potassium (K2P) channels. The inflammation of the central nervous system (CNS) impairs the olfactory function and gives rise to large amounts of extracellular ATP and adenosine, which act as pro-inflammatory and anti-inflammatory mediators, respectively. However, it is unclear whether neuronal A_1R in the olfactory bulb modulates the sensory function and how this is impacted by inflammation. Here, we show that signaling *via* neuronal A_1R is important for the physiological olfactory function, while it cannot counteract inflammation-induced hyperexcitability and olfactory deficit. Using neuron-specific A_1R-deficient mice in patch-clamp recordings, we found that adenosine modulates spontaneous dendro-dendritic signaling in mitral and granule cells *via* A_1R. Furthermore, neuronal A_1R deficiency resulted in olfactory dysfunction in two separate olfactory tests. In mice with experimental autoimmune encephalomyelitis (EAE), we detected immune cell infiltration and microglia activation in the olfactory bulb as well as hyperexcitability of mitral cells and olfactory dysfunction. However, neuron-specific A_1R activity was unable to attenuate glutamate excitotoxicity in the primary olfactory bulb neurons *in vitro* or EAE-induced olfactory dysfunction and disease severity *in vivo*. Together, we demonstrate that A_1R modulates the dendro-dendritic inhibition (DDI) at the site of mitral and granule cells and impacts the processing of the olfactory sensory information, while A_1R activity was unable to counteract inflammation-induced hyperexcitability.

Keywords: adenosine, A_1R, purinergic signaling, EAE, olfactory bulb, neuroprotection, mitral cells, olfactory dysfunction

INTRODUCTION

Adenine nucleotides are essential neurotransmitters in cellular homeostasis and disease. During synaptic transmission and also under inflammatory conditions, neurons and astrocytes can release adenosine triphosphate (ATP) (Burnstock et al., 2011). This is then rapidly degraded to adenosine diphosphate (ADP) and subsequently processed to adenosine monophosphate (AMP). and adenosine by the ectoenzymes CD39 (ectonucleoside triphosphate diphosphohydrolase-1) and CD73 (5′-ribonucleotide phosphohydrolase) (Dunwiddie et al., 1997; Sebastiao et al., 1999; Zimmermann, 2021). Extracellular adenosine binds and promotes its main cellular functions *via* the purinergic P1 receptors A_1, A_{2A}, A_{2B}, and A_3 (Fredholm et al., 2011). In the central nervous system (CNS), ample evidence suggests that the functions of adenosine are predominantly mediated by the high-affinity A_1R (Fredholm et al., 2001) as well as the $A_{2a}R$ (Gomes et al., 2011; Stockwell et al., 2017). A_1R is mainly coupled to the pertussis toxin (PTX)-sensitive G proteins of the $G_{\alpha\ i}$ and $G_{\alpha\ o}$ families of the guanine nucleotide-binding proteins (Munshi et al., 1991). Consequently, neuronal stimulation of A_1R leads to the inhibition of adenylyl cyclase (AC) and reduction of cAMP production, as well as the inhibition of the cAMP-dependent kinase (PKA), which modulates the release of neurotransmitters and neuropeptides (Carruthers et al., 2001; Jeong et al., 2003). Other targets of $G_{\alpha\ i}$ include K^+ channels (Kirsch et al., 1990; Sickmann and Alzheimer, 2003; Kim and Johnston, 2015) and Ca^{2+} channels in the CNS (Liu and Gao, 2007). Of note, stimulation of A_1R also activates the phospholipase C (PLC) pathway *via* the release of $G_{\beta\ \gamma}$ dimers in various cell types (Biber et al., 1997; Dickenson et al., 1998; Fenton et al., 2010).

Neuromodulation by adenosine is of critical importance to a wide variety of CNS functions (Gourine et al., 2009; Nazario et al., 2017; Ballesteros-Yáñez et al., 2018; Lazarus et al., 2019; Jagannath et al., 2021) and recently we also found that it is involved in olfactory information processing (Rotermund et al., 2018; Schulz et al., 2018). Olfactory signaling is provided by an interplay of several cell types. After odor detection at the site of the olfactory sensory neurons, the signal converges on glomerular columns and is processed by several inhibitory neurons, such as periglomerular interneurons and granule cells (Egger and Urban, 2006; Wachowiak and Shipley, 2006; Linster and Cleland, 2009; Burton, 2017). The projection neurons, mitral, and tufted cells integrate all inputs to create the output signal of the olfactory bulb (Geramita et al., 2016) and transmit it to higher cortical areas of the olfactory pathway, such as the anterior olfactory nucleus and the piriform and entorhinal cortices (Neville and Haberly, 2004; Isaacson, 2010; Rotermund et al., 2019). Dendrites of the mitral cells form specialized reciprocal synapses with dendrites of the glomerular interneurons and granule cells that result in a mechanism termed dendro-dendritic inhibition (DDI) (Rall et al., 1966; Isaacson and Strowbridge, 1998; Schoppa, 2006; Balu et al., 2007; Todd Pressler and Strowbridge, 2020). In the main olfactory bulb A_1R and to a less extent $A_{2A}R$ are expressed in mitral cells (Reppert et al., 1991; Lein et al., 2006; Rotermund et al., 2018). Activation of A_1R on mitral cells hyperpolarizes the cell by increasing the potassium currents through two-pore domain potassium (K2P) channels. This hyperpolarization decreases firing frequency of mitral cells at rest but has no impact on the firing frequency upon stimulation of sensory axons mimicking sensory input into the cell. Thereby, adenosine might increase the signal-to-noise-ratio detecting olfactory stimuli (Rotermund et al., 2018). In addition, adenosine inhibits L- and P/Q-type calcium channels by reducing the calcium-dependent vesicular glutamate release of mitral cells. At reciprocal synapses with GABAergic granule cells and parvalbumin interneurons, the reduced glutamate release in turn decreases DDI (Schulz et al., 2018).

During chronic autoimmune CNS inflammation, as can be detected during multiple sclerosis (MS), the olfactory function is compromised (Lucassen et al., 2016) and correlates with disease duration and severity (Yang et al., 2016; Uecker et al., 2017; Bsteh et al., 2019). Of note, olfactory dysfunction is already detectable in patients early at the onset of the disease, where the patients experience increased olfactory threshold in four out of five cases (Lutterotti et al., 2011). In primary-progressive MS (PPMS), around 84% of patients suffer from olfactory dysfunction affecting the olfactory threshold and odor identification and discrimination (Joseph and De Luca, 2016).

Disease severity in inflammatory diseases, such as MS and its animal model EAE are modulated by the extent of immune cell infiltration, immune cell composition, and their effector function (Attfield et al., 2022). Besides neuron- and glial-intrinsic properties play a major role in promoting or inhibiting neurodegeneration (Friese et al., 2014; Healy et al., 2022; Lee et al., 2022). This is particularly relevant in the progressive disease stages of MS, mirrored by the chronic phase of the EAE. In neuroinflammation glutamate, excitotoxicity is one of the main detrimental causes resulting in neurodegeneration (Woo et al., 2021). In inflammation, ATP is released into the extracellular space, where it exerts pro-inflammatory functions (Cauwels et al., 2014; Jesudasan et al., 2021). On the other hand, adenosine, as a degradation product of the enzymatic conversion of ATP by CD39 and CD73, promotes an anti-inflammatory milieu (Schetinger et al., 2007; Deaglio and Robson, 2011). Moreover, several studies indicate neuroprotective effects by adenosine in the CNS (Chen et al., 2001; Cunha, 2016; Coppi et al., 2021). However, the relative contribution of ATP- and adenosine-dependent neuronal signaling during neuroinflammation in driving or protecting against olfactory injury is unknown. Adenosine could potentially suppress neuronal excitability by restricting calcium influx and inhibiting glutamate release, eventually counteracting neuronal calcium overload (Corradetti et al., 1984; Dunwiddie et al., 1984; Pereira-Figueiredo et al., 2021). This could be mediated presynaptically, as A_1 activation inhibits voltage-activated calcium channels (Ca_v) reducing transmitter exocytosis (Banie and Nicholls, 1993; Zhu and Ikeda, 1993; Umemiya and Berger, 1994; Gundlfinger et al., 2007). In addition, the postsynaptic adenosine-induced opening of potassium channels and the consecutive hyperpolarization prevents the activation of Ca_v and stabilizes the Mg^{2+} block of NMDA receptor channels, thereby avoiding excessive neuronal calcium influx (Trussell and Jackson, 1985;

de Mendonça et al., 1995). Accordingly, ischemia-induced synaptic depression is substantially reduced in the hippocampal slices of A_1-deficient mice (Johansson et al., 2001; Kawamura et al., 2019). Similarly, A_1-deficient mice show an ameliorated disease course of experimental autoimmune encephalomyelitis (EAE) (Tsutsui et al., 2004), the animal model of MS. However, these EAE experiments used constitutive A_1-deficient mice of the entire organism and did not allow to distinguish A_1-dependent functions of immune cells from those of inflamed neurons. Here, we set out to disentangle the role of neuronal A_1R purinergic signaling in the olfactory bulb under healthy and inflammatory conditions. In healthy conditions, patch clamp recordings of olfactory bulb mitral and granule cells showed A_1R-dependent modulation of dendro-dendritic signaling, and a lack of A_1R expression in neurons impaired the performance of the animals in olfactory behavior tests. During neuroinflammation, the gain of the current–frequency relationship of mitral cells increased, yet A_1R deficiency neither modulated this rise in gain nor the extent of neurodegeneration or impaired the olfactory performance.

RESULTS

Neuronal Adenosine 1 Receptor in Homeostatic Conditions

To disentangle the olfactory role of the neuronal A_1 receptor in health and neuroinflammation, we first generated a neuron-specific A_1R-deficient mouse line. We bred mice with a floxed *Adora1* gene, which encodes for A_1R (Scammell et al., 2003), with mice that express the Cre recombinase driven by the SNAP25 promoter (Zitman and Richter-Levin, 2013). By further breeding the $A_1R^{flx/flx}$;$SNAP25^{Cre}$ mice to *tagger* mice (Tag) that contain a Cre-dependent nuclear fluorescent tag as well as an HA tag (Kaczmarczyk et al., 2019), we could visualize neuron-specific expression in almost all brain regions, including the olfactory bulb (**Figure 1A**), cortex, hippocampus, and the spinal cord (**Supplementary Figures 1A–C**). Validation of reporter expression in specific neuronal subsets in the olfactory bulb revealed labeling of approximately 80% of NeuN-positive neurons in the granular cell layer and slightly fewer in the glomerular layer of the main olfactory bulb (data not shown) and 87% of the reelin-positive mitral cells in the mitral cell layer (**Supplementary Figure 1D**). Specific labeling of neurons using the $SNAP25^{Cre}$ mouse was confirmed by the staining of glial markers Iba1 (microglia), GFAP (astrocytes), and CNPase (oligodendrocytes) (**Supplementary Figures 1E–G**). While *Adora1* expression was unaltered in the spleen in qPCR (**Figure 1B**), *Adora1* expression was significantly reduced in the olfactory bulb tissue of $A_1R^{flx/flx}$;$SNAP25^{Cre}$ suggesting a neuron-specific knockout (n = 3 per group, **Figure 1B**). In addition, we confirmed a reduction of A_1R in primary cell cultures by immunocytochemistry (n = 8 per group in n = 4 biological replicates, **Supplementary Figure 1H**). In contrast, mRNA expression levels of the P1 receptors A_{2a} (*Adora2a*), A_{2b} (*Adora2b*), and A_3 (*Adora3*) did not differ in the olfactory bulb tissue of A_1R-deficient mice compared to their wildtype littermates, suggesting no relevant compensatory mechanisms in the transcriptional levels in these mice (n = 3 per group, **Figure 1C**).

By comparing $A_1R^{flx/flx}$ and $A_1R^{flx/flx}$;$SNAP25^{Cre}$ we did not observe apparent phenotypic alterations, including body weight (**Supplementary Figure 1I**). However, neuron-specific A_1R deficiency resulted in slightly reduced survival rate of $A_1R^{flx/flx}$;$SNAP25^{Cre}$ mice compared to their floxed littermates. At 15 weeks of age, 7% of $A_1R^{flx/flx}$;$SNAP25^{Cre}$ mice showed unexpected death while only 3% of $A_1R^{flx/flx}$ mice (**Supplementary Figure 1J**) died. Moreover, neuronal cell count in the olfactory bulbs of wildtype and A_1R knockout mice showed no differences in mitral cell counts, (**Figure 1D**), suggesting no overt developmental differences. Thus, having a validated neuron-specific A_1R-deficient mouse line enabled us to disentangle the role of the neuronal A_1R function in health and in neuroinflammation.

Since we previously showed that activation of A_1R in mitral cells led to an increase of background potassium conductance by two-pore-domain potassium channel subfamily (K2P) (Rotermund et al., 2018), we interrogated whether $A_1R^{flx/flx}$;$SNAP25^{Cre}$ shows a functional abrogation in whole-cell recordings of mitral cells in olfactory bulb slices. Application of adenosine induced an outward shift of the holding current in $A_1R^{flx/flx}$ animals (23 $\pm$ 2 pA, n = 7) but failed to increase the background current in the mitral cells of $A_1R^{flx/flx}$;$SNAP25^{Cre}$ mice (n = 5) (**Figure 1E**). Next, we examined whether the lack of A_1R in mitral cells has an impact on neuronal properties of mitral cells. Consistent with the data of global A_1R knockout mice (Johansson et al., 2001), we did not find a significant difference in the resting membrane potential (-41.4 ± 0.8 mV in $A_1R^{flx/flx}$ vs. -44.5 ± 2.1 mV in $A_1R^{flx/flx}$;$SNAP25^{Cre}$) (**Supplementary Figure 2A**) or input resistance (165 $\pm$ 23 MΩ in $A_1R^{flx/flx}$ vs. 179 $\pm$ 40 MΩ in $A_1R^{flx/flx}$;$SNAP25^{Cre}$) of the recorded cells (**Figure 1F**). Stepwise increase of the commando potential and the recording of the corresponding whole-cell conductance to illustrate the current–voltage relationship also did not reveal any differences between A_1R-proficient and A_1R-deficient mitral cells (**Supplementary Figure 2B**). To analyze potential differences in firing behavior, we applied depolarizing current injections of consecutively higher amplitude and plotted the frequency of the induced action potentials of mitral cells. Neither the rheobase, the first current step resulting in a membrane depolarization beyond the action potential threshold (**Supplementary Figure 2C**), nor the progression of the F/I plot showed significant alterations in the excitability of $A_1R^{flx/flx}$;$SNAP25^{Cre}$ mitral cells in comparison to the A_1R-proficient cells (**Figure 1G**). Hence, while membrane properties of mitral cells in $A_1R^{flx/flx}$;$SNAP25^{Cre}$ seem unaltered, mitral cells show a profound deficit in response to extracellular adenosine concentrations with K2P activation.

Neuronal Adenosine 1 Receptor Is Involved in Olfactory Dendro-Dendritic Transmission

Having shown the A_1R-dependent modulation of presynaptic calcium channels in mitral cells (Schulz et al., 2018), we next investigated the structural and functional role of A_1R on synaptic

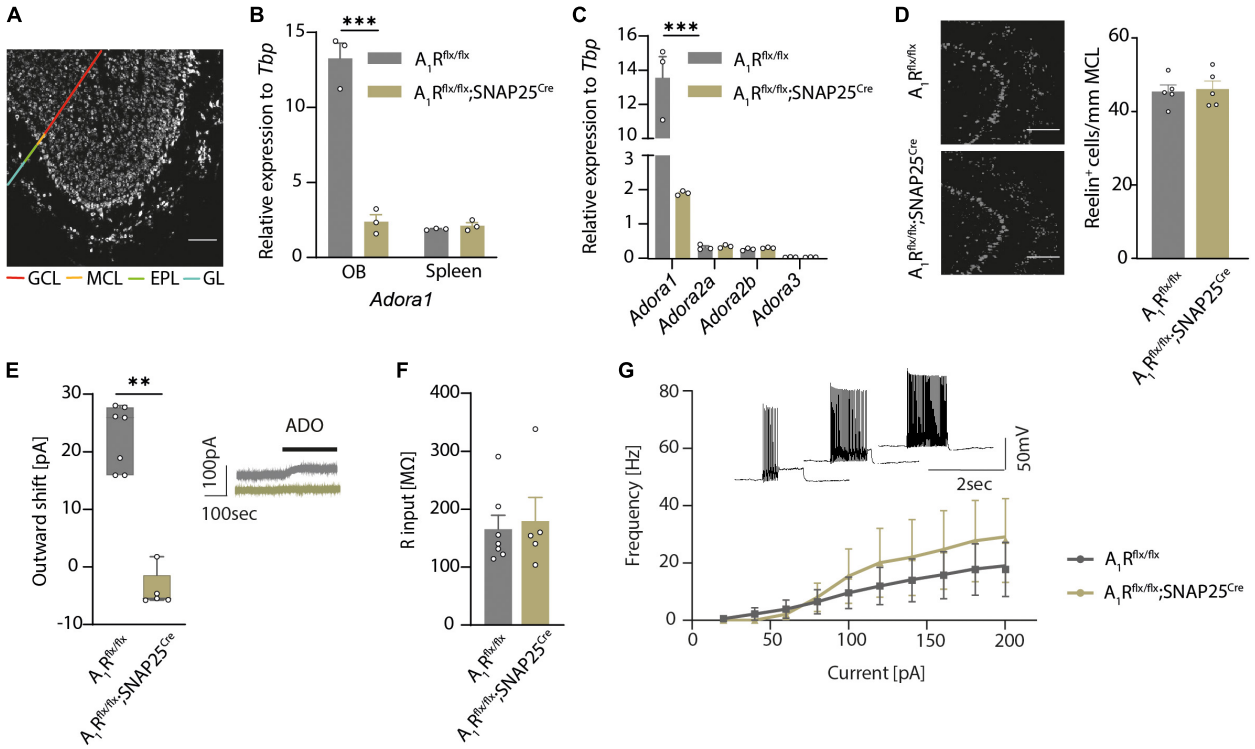

FIGURE 1 | $A_1R^{flx/flx}$;SNAP25^{Cre} results in neuron-specific A1R knockout. **(A)** HA-tagged reporter expression in neuron-specific A_1R knockout mouse line $A_1R^{flx/flx}$;Tag;SNAP25^{Cre} indicates wide distribution of Cre expression in the main olfactory bulb. Representative image shows a sagittal view of the main olfactory bulb comprising the granular cell layer (GCL), internal plexiform layer (not marked), mitral cell layer (MCL), external plexiform layer (EPL), and the glomerular layer (GL) as indicated by different colors. HA-tag was stained with anti-HA antibody. **(B)** Quantitative qPCR of *Adora1* (coding for the A_1R) mRNA expression of olfactory bulbs and spleens (BF_{10} = 0.538) isolated from $A_1R^{flx/flx}$ (n = 3) and $A_1R^{flx/flx}$;SNAP25^{Cre} (n = 3). **(C)** Quantitative qPCR mRNA expression of P1 receptor genes *Adora1*, *Adora2a* (BF_{10} = 0.646), *Adora2b* (BF_{10} = 0.624), and *Adora3* (BF_{10} = 0.565) in the olfactory bulb of $A_1R^{flx/flx}$ (n = 3) and $A_1R^{flx/flx}$;SNAP25^{Cre} (n = 3) mice. **(D)** Mitral cells analyzed by marker Reelin in the mitral cell layer in $A_1R^{flx/flx}$ (n = 5) and $A_1R^{flx/flx}$;SNAP25^{Cre} (n = 5) mice (BF_{10} = 0.337). **(E)** Outward shift of the holding current in the mitral cell patch clamp recordings evoked by the application of 100 μM of adenosine (ADO) in $A_1R^{flx/flx}$ (n = 7 slices from 5 mice) and $A_1R^{flx/flx}$;SNAP25^{Cre} (n = 5 slices from 4 mice) (MWU; U = 0, P = 0.0025). Representative traces in gray ($A_1R^{flx/flx}$) and olive ($A_1R^{flx/flx}$;SNAP25^{Cre}). **(F)** Input resistance was measured in patch clamp recordings of mitral cells from $A_1R^{flx/flx}$ (n = 7 slices from 5 mice) and $A_1R^{flx/flx}$SNAP25^{Cre} (n = 5 slices from 4 mice) mice, BF_{10} = 0.486. **(G)** Progression of the F/I plot shows excitability of mitral cells from $A_1R^{flx/flx}$ (n = 7 slices from 5 mice) mice vs. $A_1R^{flx/flx}$;SNAP25^{Cre} (n = 5 slices from 4 mice) (BF_{10} = 0.480-0.537). Data points display mean ± s.e.m. $^{**}P < 0.01$, $^{***}P < 0.001$.

connections of mitral cells in the external plexiform layer. Here mitral cells are forming dendro-dendritic synapses with several GABAergic interneurons, mainly granular cells. These reciprocal connections are involved in recurrent and lateral inhibition of excited mitral cells by granule cells (Isaacson and Strowbridge, 1998; Egger and Kuner, 2021). Schematic representation is shown in **Figure 2A**. Neuronal A_1R deficiency resulted in a reduced density of glutamatergic synapses as recorded by synapsin1 and PSD-95 expression and colocalization (n = 6 per group, **Figures 2B,C**). Yet, inhibitory synapses in the external plexiform layer were not significantly affected (**Supplementary Figure 2D**). As this reciprocal connection of mitral cells with modulating granular cells seems to be affected by the lack of the A_1R, we further investigated the synaptic functions by patch-clamp recordings.

By recording spontaneous inhibitory and excitatory synaptic currents (sPSCs) in granule cells using high chloride intracellular solution, we revealed a lower frequency of inputs in $A_1R^{flx/flx}$;SNAP25^{Cre} animals compared to $A_1R^{flx/flx}$ controls (47.61 ± 11.37, n = 10, vs. 158.19 ± 32.61, n = 10, mean summarized number of inputs per minute, **Figure 2D**). In contrast, recording sPSCs in mitral cells revealed no differences in the baseline activity (1326 ± 253 in $A_1R^{flx/flx}$, n = 9, vs. 1559 ± 291 in $A_1R^{flx/flx}$;SNAP25^{Cre}, n = 8, mean summarized number of inputs per minute) in the recorded sample (**Figure 2E**). Application of 100 μM of adenosine significantly reduced sPSC frequency in the granule cells of $A_1R^{flx/flx}$ animals by 36.91 ± 5.74% (n = 10), whereas in the granule cells of $A_1R^{flx/flx}$;SNAP25^{Cre} sPSC frequency did not change upon adenosine application compared to baseline values (frequency elevated to 7.9 ± 11%, n = 10), confirming the absence of A_1R-induced effects in the A_1R knockout. Concomitantly, wildtype mitral cells showed a significant reduction of synaptic input frequency upon the application of 100 μM of adenosine (28.6 ± 7.8%, n = 9) but not the mitral cells of $A_1R^{flx/flx}$ SNAP25^{Cre} animals (frequency lowered by 6.7 ± 5.4%, n = 9)

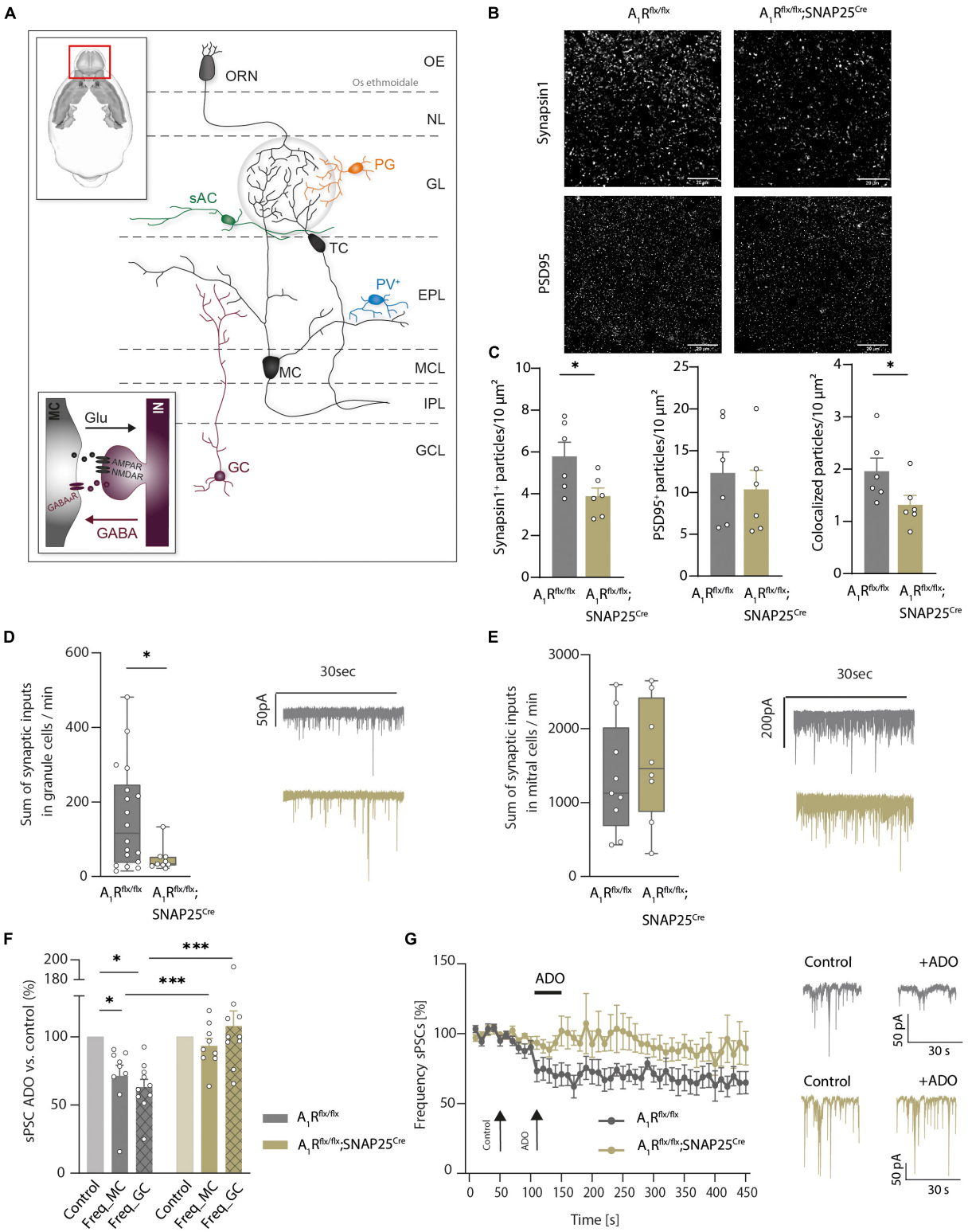

FIGURE 2 | Adenosine modulates microcircuits in the external plexiform layer of the main olfactory bulb *via* A_1R. **(A)** Schematic presentation of main olfactory bulb with principal neurons (MC, TC) and local interneurons [periglomerular neurons (PG), short axon cells (sAC), parvalbumin neurons (PV), and granule cells (GC)]. Inset: Mechanism of dendro-dendritic signaling at the reciprocal MC-GC synapse. **(B)** Representative images of synaptic density in the external plexiform layer (EPL) of the

(Continued)

FIGURE 2 | main olfactory bulb in A_1R-proficient ($A_1R^{flx/flx}$) and A_1R-deficient ($A_1R^{flx/flx}$;$SNAP25^{Cre}$) mice. Immunohistochemical stainings comprised the presynaptic protein synapsin1 and the postsynaptic protein PSD95. **(C)** Immunohistochemical analysis of synapsin1, PSD95 (BF_{10} = 0.518), and co-expression of synapsin1 and PSD95 in the EPL in $A_1R^{flx/flx}$ and $A_1R^{flx/flx}$;$SNAP25^{Cre}$ (n = 6 per group). **(D)** Whole cell current recordings of granule cells. Number of synaptic inputs quantified as the sum of sPSC events per minute in $A_1R^{flx/flx}$ (n = 18) compared to $A_1R^{flx/flx}$;$SNAP25^{Cre}$ (n = 9). MWU; U = 40, P = 0.035. **(E)** Whole cell current recordings of mitral cells. Number of synaptic inputs quantified as the sum of sPSC events per minute ($A_1R^{flx/flx}$ n = 9; $A_1R^{flx/flx}$;$SNAP25^{Cre}$ n = 8), BF_{10} = 0.476. **(F)** Frequency of sPSCs in mitral cells and granule cells after the application of 100 μM of adenosine (mean of second 130–170 of recording) compared to baseline (mean of second 30–70 of recording) in $A_1R^{flx/flx}$ (n = 10 in granule cells, n = 9 in mitral cells) and $A_1R^{flx/flx}$;$SNAP25^{Cre}$ (n = 10 in granule cells, n = 9 in mitral cells). Adenosine-dependent effect on sPSC frequency was analyzed by the Wilcoxon ranking test. For A1R-proficient cells, P = 0.00195 (granule cells) and P = 0.00391 (mitral cells); for A1R-deficient cells, BF_{10} (paired test) = 0.322 (granule cells) and BF_{10} (paired test) = 0.793 (mitral cells). Genotype comparison was done by Mann–Whitney U test. Adenosine effect $A_1R^{flx/flx}$ vs. $A_1R^{flx/flx}$;$SNAP25^{Cre}$ for granule cells (U = 6, P = 0.003) and mitral cells (U = 15, P = 0.024). **(G)** Frequency of sPSCs in mitral cells normalized to baseline over the time course of >7 min. Representative traces showing sPSC of mitral cells under baseline condition and after treatment with 100 μM of adenosine at timespoints indicated by arrows. $^*P < 0.05$, $^{***}P < 0.001$.

(**Figure 2F**). Time course analysis confirmed the reduction of synaptic input frequency by adenosine in A_1R-proficient, but not in A_1R-deficient mitral cells over at least 6 min (**Figure 2G**). Taken together, these data corroborate the A_1R-dependent modulation of dendro-dendritic circuits by adenosine.

Neuronal Adenosine 1 Receptor Is Critical for Olfactory Function

As A_1R is important for the DDI of mitral cells, we next explored whether that translates to an olfaction phenotype using a two-sided olfactory detection test with the odor of vanilla and almond (**Figure 3A**). During the first trial (when no odor was presented), mice of both genotypes (n = 10 per group) spent the same amount of time sniffing at the two openings at the left and right sides of the cage (**Figure 3B**) and did not show differences in rearing events, which reflects a similar exploratory behavior (**Figure 3C**). Thus, neuronal A_1R deletion did not affect the general exploratory and sniffing behavior, and there was no bias toward one side of the cage. In trial 2, an unfamiliar odor (vanilla) was presented at the right side of the cage (**Figure 3B**). Whereas $A_1R^{flx/flx}$ control mice preferentially sniffed at the opening with vanilla, $A_1R^{flx/flx}$;$SNAP25^{Cre}$ did not display a preference for the new odor (**Figure 3B**). In trial 3, we introduced the odor almond at the side opposite vanilla (**Figure 3A**). We used almond as a new odor with the expectation that mice would investigate it more intensely than the already familiar vanilla. However, all mice spent only few seconds sniffing it, indicating that almond flavor induced an aversive reaction, at least under these experimental conditions (**Figure 3B**). Whereas these results suggest that neuronal A_1R deficiency impairs olfaction; we cannot exclude that an altered novelty-induced behavior of the $A_1R^{flx/flx}$;$SNAP25^{Cre}$ mice caused a lack of preference for the new odor of vanilla. We thus tested olfaction in a task that relies on an innate behavior to 2,5-dihydro-2,4,5-trimethylthiazoline (TMT), a constituent of fox urine and feces (Saito et al., 2017). In this task, the neuronal A_1R-deficient mice (n = 6) showed reduced TMT-induced freezing compared to control mice ($A_1R^{flx/flx}$ n = 11, **Figure 3D**). Freezing behavior enhanced during the trial because TMT concentration at the bottom of the cage increased with time. While this pattern was observed in both genotypes, the time-dependent increase in freezing was less pronounced in the $A_1R^{flx/flx}$;$SNAP25^{Cre}$ animals compared to control littermates (effect of the genotype × time interaction, F = 5.23; P = 0.032). Thus, neuronal A_1R deficiency reduces olfaction-controlled behaviors in two paradigms based on unrelated behavioral functions. To exclude that neuronal A_1R deficiency might have indirectly influenced olfaction tasks by altering behavioral functions, we tested $A_1R^{flx/flx}$;$SNAP25^{Cre}$ mice and $A_1R^{flx/flx}$ littermates in an open field and elevated plus-maze test. However, no differences were detected between genotypes in either test (**Supplementary Figures 3A–I**), indicating that neuronal A_1R alters olfaction but not novelty-induced anxiety and exploration.

Neuroinflammation Leads to Mitral Cell Hyperexcitability That Is Not Modulated by Neuronal Adenosine 1 Receptor

We demonstrated that mitral cells of the olfactory bulb express A_1R and their activation leads to hyperpolarization (Rotermund et al., 2018) and reduction of calcium influx and glutamate release (Schulz et al., 2018). To dissect whether A_1R-dependent effects could potentially counteract excessive glutamate release, hyperexcitability, and neuronal injury during neuroinflammation, we utilized primary cultures of olfactory bulb neuronal cells of A_1R-proficient and A_1R-deficient embryos. We detected *Adora1* expression by qRT-PCR in olfactory bulb primary neurons during neuronal differentiation at days *in vitro* (DIV) 7, 14, and 21 showing the peak of expression after 14 days (n = 3 per group, **Supplementary Figure 4A**). Furthermore, we confirmed the lack of *Adora1* transcripts in neuronal cultures dissected from $A_1R^{flx/flx}$;$SNAP25^{Cre}$ compared to wild types ($A_1R^{flx/flx}$) (n = 3 per group, **Figure 4A**). We confirmed the results by demonstrating a significant reduction of immunofluorescence A_1R staining in $A_1R^{flx/flx}$;$SNAP25^{Cre}$ in comparison to wildtype cultures (n = 4 biological replicates per group with two technical replicates each, **Supplementary Figure 4B**). Upon the application of glutamic acid, neuronal survival was reduced to a similar extent in wildtype and $A_1R^{flx/flx}$;$SNAP25^{Cre}$ cultures as measured by counting MAP2-positive neurons (n = 3 biological replicates with 2–3 technical replicates, **Figure 4B**). By measuring the cell viability longitudinally over 15 h using a bioluminescence method (Realtime glo, Promega®), glutamic acid treatment led to a decrease irrespective of the genotype (n = 4 biological replicates per group with at least 5 technical replicates each, **Figure 4C**). Similar results were obtained by applying the A_1R agonist 2-chloro-N6-cyclopentyladenosine (CCPA) to wildtype neuronal cultures (n = 4 biological replicates with at least 5 technical replicates each, **Supplementary Figure 4C**).

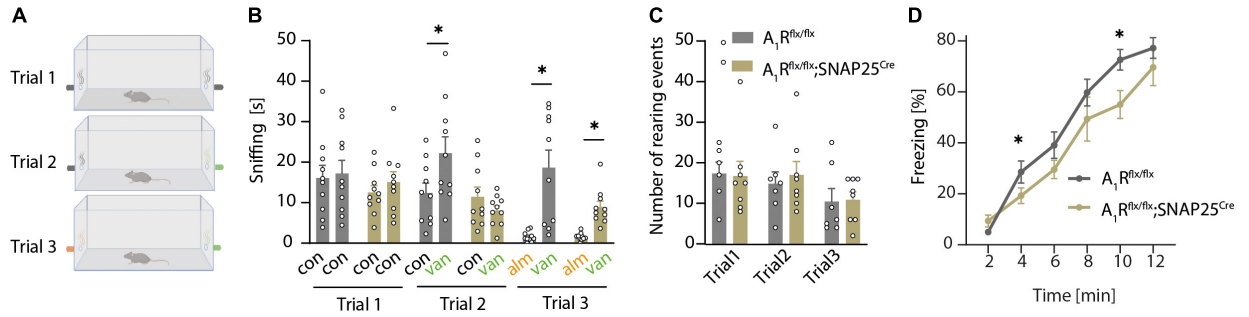

FIGURE 3 | A_1R deficiency results in olfactory dysfunction. **(A)** Graphical workflow of olfactory detection test. $A_1R^{flx/flx}$ and $A_1R^{flx/flx}$;$SNAP25^{Cre}$ were exposed to empty tubes (black), or tubes perfumed with a concentrate of vanilla (green) or almond (orange). Each trial lasted 4 min. **(B)** Quantification of olfactory detection tests. Preference to new odor analyzed by the time of sniffing at the respective side (s) (n = 10 per group, BF_{10} = 0.361). **(C)** Events of rearing during each trial in olfactory detection test of $A_1R^{flx/flx}$ and $A_1R^{flx/flx}$;$SNAP25^{Cre}$ mice (BF_{10} = 0.439–0.473). **(D)** TMT-based olfactory test. Time of freezing in percent in bins of 2 min in $A_1R^{flx/flx}$ (n = 11) and $A_1R^{flx/flx}$;$SNAP25^{Cre}$ (n = 6). Bonferroni *post-hoc* test after a mixed multifactorial ANOVA; *$P < 0.05$.

Next, we asked whether the A_1R network of the olfactory bulb modulates neuronal survival during neuroinflammation in the EAE mouse model. However, $A_1R^{flx/flx}$;$SNAP25^{Cre}$ mice did not show a different disease course (n = 18 per group, **Figure 4D**), area under the curve (**Figure 4E**), onset (**Supplementary Figure 4D**), or final score at day 30 post-immunization (p.i.) (**Supplementary Figure 4E**) in comparison to $A_1R^{flx/flx}$ littermate control mice. Also, on a neuropathological level, neither the microglial activation nor the amount of immune cell infiltration of T cells differed in the olfactory bulbs of the two genotypes in the chronic phase of EAE (n = 5 per group, **Figures 4F,G**). We could also not detect the differences between the genotypes in the counts of Reelin-positive neurons in the mitral cell layer (n = 5 per group, **Figure 4H** and **Supplementary Figure 4F**) or NeuN-positive cells (mostly adult neurons; **Supplementary Figure 4G**) in all the recorded layers at day 15 p.i. or at day 30 p.i. of EAE.

Since the clinical EAE score mainly reflects motor disabilities due to inflammation-induced injury of the spinal cord, we next tested whether inflammation functionally impairs olfaction. Thus, we assessed the animals in olfactory behavior using the odor detection test ($A_1R^{flx/flx}$ n = 6 and $A_1R^{flx/flx}SNAP25^{Cre}$ n = 7, **Figure 4I**) and the TMT-based olfactory test ($A_1R^{flx/flx}$ n = 10 and $A_1R^{flx/flx}$;$SNAP25^{Cre}$ n = 8, **Figure 4J**). We tested the animals at the early phase (EAE day 10–12 p.i.) of the disease to avoid paralysis-associated immobility which could compromise testing. Of note, in contrast to the reduced sensory performance of healthy neuron-specific A_1R-deficient animals in olfactory tests, we detected no differences between A_1R-deficient and wildtype EAE mice in their ability to detect the odor of vanilla and almond in the olfactory detection test (**Figure 4I**) and in their freezing response in TMT-based olfactory testing during EAE (**Figure 4J**). Neuroinflammation impaired olfactory function in the A_1R-proficient mice in comparison to healthy condition (healthy n = 11, EAE n = 10) but was not further modulated in the A_1R-deficient mice $A_1R^{flx/flx}$;$SNAP25^{Cre}$ (healthy n = 6, EAE n = 8, **Figure 4K**).

As extracellular concentrations of ATP and adenosine are elevated during inflammatory conditions (Cauwels et al., 2014; Di Virgilio et al., 2020), we explored a possible functional impact of A_1R on excitability during inflammatory conditions, the acute phase of the EAE model. The analysis of mitral cell membrane parameters by patch-clamp recordings revealed an increase in the slope of the F/I plot in the brain slices of diseased animals (EAE day 13–16 p.i.) indicating higher excitability of the neurons in the inflammatory environment (**Figures 4L,M**). This increase, however, did not differ between $A_1R^{flx/flx}$;$SNAP25^{Cre}$ and $A_1R^{flx/flx}$ controls, arguing against a pivotal role of neuronal A_1R in controlling mitral cell excitability during inflammation (**Figure 4M**). In addition, we could not reveal an altered resting membrane potential (**Supplementary Figure 4H**), rheobase (**Supplementary Figure 4I**), or modulation of adenosine-induced outward current (**Supplementary Figure 4J**) due to neuroinflammation in both genotypes (measured at the acute phase of EAE day 13–16 p.i.). Taken together, we could detect inflammation-induced olfactory impairment and hyperexcitability that is, however, not functionally counteracted by A_1R.

DISCUSSION

Adenosine is an important neuromodulator of intercellular communication in the olfactory bulb and is also involved in inflammatory conditions (Fredholm, 2014; Liu and Xia, 2015; Santiago et al., 2020). Here, we investigated to what extent the olfactory bulb is sensitive to inflammation-induced neurodegeneration and whether neuronal function, cellular integrity, and olfactory behavior can be modulated by the activity of A_1R.

In our previous study (Schulz et al., 2018), we already demonstrated that constitutive A_1R-deficient animals perform differently than wildtype animals in an olfactory-guided behavior test. Since adenosine is a powerful modulator of metabolism, such as thermoregulation and obesity (Carlin et al., 2018; Futatsuki et al., 2018; Gnad et al., 2020), we could not exclude that the observed difference in the buried food test was due to an altered metabolic state with different motivation of

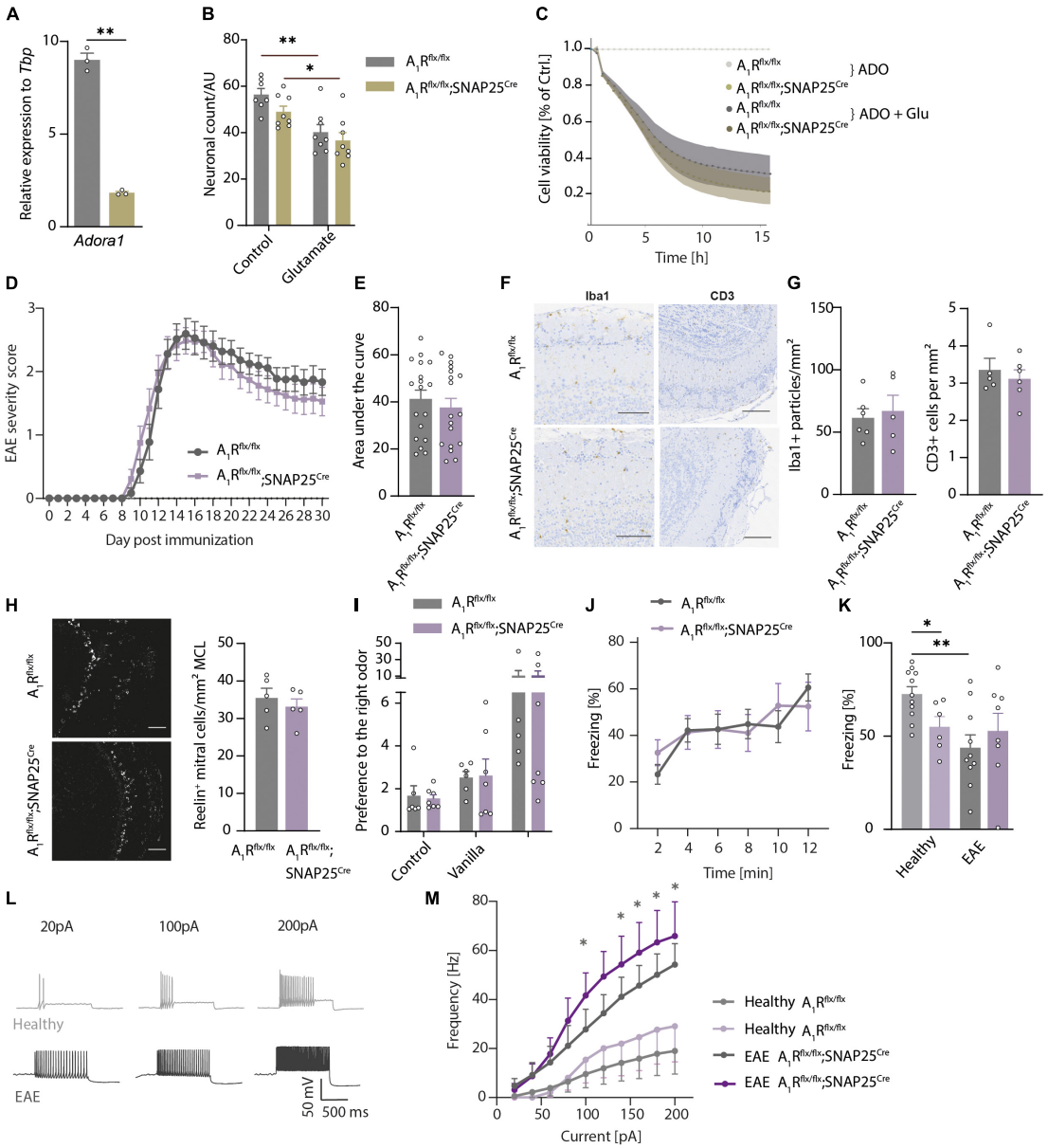

FIGURE 4 | Neuroinflammation results in olfactory dysfunction and hyperexcitability that is not influenced by neuronal A_1R. **(A)** *Adora1* expression in primary neuronal cultures of olfactory bulb neurons DIV 14–16 of $A_1R^{flx/flx}$ (gray) and $A_1R^{flx/flx}$;$SNAP25^{Cre}$ (beige) ($n = 3$ per group). **(B)** Neuronal survival *in vitro* measured by MAP2-positive cells after treatment with 5 μM of glutamate for 6 h in $A_1R^{flx/flx}$ and $A_1R^{flx/flx}$;$SNAP25^{Cre}$ ($n = 3$ biological replicates with 2–3 technical replicates). **(C)** Luminescence-based measurement of cell viability over 15 h treated with 10 μM of adenosine (ADO) and 5 μM of glutamate or medium as control ($n = 4$ biological replicates per group with at least 5 technical replicates each). **(D)** Clinical time course of experimental autoimmune encephalomyelitis (EAE) over 30 days ($n = 18$ per group) in A_1R-proficient ($A_1R^{flx/flx}$) and A_1R-deficient ($A_1R^{flx/flx}$;$SNAP25^{Cre}$) mice. **(E)** Disease severity in EAE analyzed by area under the curve ($BF_{10} = 0.384$). **(F)** Representative images and **(G)** quantification of microglia activation measured by Iba1 ($BF_{10} = 0.506$), and T-cell infiltration evaluated by CD3-positive cells/mm^2 ($BF_{10} = 0.476$) in the main olfactory bulb in coronal slices ($n = 5$ per group). **(H)** Reelin-positive mitral cells per mm mitral cell layer at day 30 post-immunization (p.i.) ($n = 5$ per group, $BF_{10} = 0.673$). **(I)** Olfactory detection test at the early phase of EAE (day 10–12 p.i.) in $A_1R^{flx/flx}$ $n = 6$ and $A_1R^{flx/flx}SNAP25^{Cre}$ $n = 7$. As mice were exposed to odors at two sides of the cage (first trial empty control, second trial vanilla on the right side, third trial almond on the left side where vanilla was reintroduced on the right side), preference to one side of the cage has been measured by means of the ratio between the sides. **(J)** TMT-based olfactory testing measured by the percentage of freezing in bins of 2 min in EAE ($A_1R^{flx/flx}$ $n = 10$ and $A_1R^{flx/flx}$;$SNAP25^{Cre}$ $n = 8$). **(K)** TMT-based olfactory behavioral test in healthy animals and at the early phase of EAE. Percentage of freezing after 10 min in $A_1R^{flx/flx}$ (healthy $n = 11$ in light gray, EAE $n = 10$ in gray) and $A_1R^{flx/flx}$;$SNAP25^{Cre}$ mice (healthy $n = 6$ in light lavender, EAE $n = 8$ in lavender). **(L)** Representative traces of mitral cell action potentials in healthy control (light gray) and acute phase of EAE (dark gray). **(M)** Increase of frequency of action potentials of mitral cells depending on the injected current in healthy ($n = 7$) and acute EAE ($n = 5$) slice preparations of $A_1R^{flx/flx}$ (healthy $n = 7$; EAE $n = 5$) and $A_1R^{flx/flx}$;$SNAP25^{Cre}$ (healthy $n = 5$; EAE $n = 7$) mice, analyzed by Mann–Whitney *U*-test. Statistical analysis was performed by two-way ANOVA in repetitive measurements **(C,D,J,L,M)** and unpaired *t*-test, if not stated otherwise; $^*P < 0.05$, $^{**}P < 0.01$.

the animals to gather food. In contrast, the olfactory tests in the present study with neuron-specific A_1R-deficient mice enabled us to show the importance of neuronal A_1R for the olfactory sensory pathway with non-food-related olfactory tests. As the Snap25 promotor was used to drive Cre expression in neurons that is widely expressed throughout the brain, we cannot completely exclude the impact of other brain regions interconnected with the olfactory sensory pathway on olfactory behavior in this study. However, we used two different olfactory tests to confirm the specificity of the A_1R effect on olfaction. The odor TMT has been used in several studies and the circuits activated by this odor are well understood (Kobayakawa et al., 2007; Saito et al., 2017; Sakano, 2020). We also excluded confounding changes in anxiety and curiosity in the neuron-specific A_1R-deficient mice that confirmed previous results using global A_1R-deficient mice (Chasse et al., 2021), whereas other studies have reported increased anxiety in A_1R-deficient mice (Johansson et al., 2001; Giménez-Llort et al., 2002).

On the cellular level, immunostainings showed a reduced number of glutamatergic synapses in the external plexiform layer, and recordings of spontaneous PSCs in granule cells revealed a lower input frequency in the $A_1R^{flx/flx}$;$SNAP25^{Cre}$ mice. The main driver of granule cell activity is glutamate release from mitral and tufted cells (Egger and Urban, 2006; Schoppa, 2006), albeit granule cells also receive GABAergic inputs from different intra-bulbar sources, such as deep short axon cells and blanes cells or from the cortical feedback projections (Pressler and Strowbridge, 2006; Boyd et al., 2012; Nunez-Parra et al., 2013). However, since most of the inputs recorded in mature granule cells are excitatory (Carleton et al., 2003), we presume that the reduction of the number of postsynaptic currents in A_1R-deficient granule cells is likely caused by a lack of glutamatergic synapses. However, we cannot entirely rule out a reduction of GABAergic inputs in knockout animals. Recent data describe $A_{2A}R$-dependent development of GABAergic synapses in the hippocampal neurons (Gomez-Castro et al., 2021), implying a role of adenosine signaling not only in homeostatic plasticity but also during neurodevelopment. Whether the observed alteration in synaptic connections in the external layer of the olfactory bulb is due to an imbalance of adenosine signaling during the development has to be determined. However, we could not find pronounced differences in the membrane properties of mitral cells in neuron-specific A_1R-deficient mice in comparison to wildtype controls. The application of adenosine was able to reduce spontaneous synaptic transmission in wildtype animals but not in A_1R-deficient mice, as shown by the recordings of postsynaptic currents in the mitral cells and granule cells. The majority of synaptic connections in the olfactory bulb circuitry are formed between the principal neurons and axonless GABAergic interneurons, such as periglomerular cells, granule cells, and parvalbumin cells and therefore are reciprocal dendro-dendritic synapses (Crespo et al., 2013; Burton, 2017; Li et al., 2020). Consistent with our previous studies showing that neuronal A1R expression is restricted to mitral and tufted cells in the olfactory bulb and that the recurrent DDI of mitral cells by granule cells and parvalbumin interneurons is reduced by A_1R signaling (Schulz et al., 2018), we conclude that adenosine modulates recurrent MC-GC synapses. However, an impact on other cell types and synapses in the circuitry cannot be ruled out. As inhibitory circuits play an important role in shaping odor representation in the olfactory bulb (Burton, 2017), alterations at this level of processing could impact olfactory function. Indeed, direct evidence for the impact of DDI on olfactory behavior exists for the granule cell–mitral cell interaction (Abraham et al., 2010; Kato et al., 2013; Miyamichi et al., 2013; Nunes and Kuner, 2015, 2018). Neuronal A_1R-deficient mice showed olfactory dysfunction as shown in our two-sided odor exposition test using the odors of vanilla and almond. Of note, mice showed avoidance behavior when exposed to almond independent of their genotype. The aversive effect could have been caused by high concentrations of the almond flavor (Yang and Crawley, 2009; Islam et al., 2018). As both, wildtype littermates and $A_1R^{flx/flx}$;$SNAP25^{Cre}$ mice avoided the almond flavor, this suggested that neuronal A1R deletion impairs but does not abolish olfaction.

Notably, neuroinflammation results in neuronal injury that not only manifests as motor but also as olfactory dysfunction. In the TMT-based olfactory test, the EAE model reproduces human MS in which olfactory dysfunctions have been recorded (Goektas et al., 2011; Schmidt et al., 2017). The olfactory detection test however, exhibited high variability in preference to the odor in the EAE group in comparison to the healthy group and to the TMT-based analysis. We also reveal a hyperexcitability of mitral cells in EAE animals at the cellular level. Inflammation not only induces excitotoxicity by increasing the glutamatergic neurotransmission and concomitantly inducing the calcium overload of neurons, but also affects the expression and function of different classes of ion channels regulating the cellular ionic homeostasis (Friese et al., 2014). RNA expression data in MS brains indicate the dysregulation of a multitude of ion channels in inflamed brain areas, among those two-pore potassium channel TREK2, voltage-activated sodium channels Nav1.2 (Schattling et al., 2016), potassium channels Kv11.3 (erg), and calcium-activated potassium channel $K_{Ca}2.3$ (Boscia et al., 2021). This could thereby affect all facets of neuronal homeostasis from resting membrane potential generation to action potential initiation and propagation. Since we blocked glutamate receptors during the examination of mitral cell excitability, we assume that the increase in gain in cells from EAE animals is not due to an acute increase of glutamatergic transmission but rather results from chronic inflammation-induced dysregulation of mitral cell ion channels. However, apart from the hyperexcitability, we could not find other apparent alterations in physiological parameters, such as resting membrane potential or whole cell currents in our recordings.

As inflammation is linked to increased concentrations of extracellular ATP and adenosine (Di Virgilio et al., 2020), purinergic receptor-mediated signaling could be involved in the modulation of neurodegeneration. Thus, A_1R-dependent signaling in neurons has the potential to counteract hyperexcitability and excitotoxicity, as its activity results in hyperpolarization and inhibition of calcium-entry *via* Ca_v (Schampel and Kuerten, 2017). However, our *in vitro*

studies with olfactory bulb neurons from neuron-specific A_1R-deficient animals and respective controls, as well as activation of the neuronal A_1R failed to rescue neurons from glutamate excitotoxicity. In contrast, the overexpression of A_1R in neurons by transfection had a positive effect on cell survival in an NMDA-based excitotoxicity assay (Serchov et al., 2012). Expression changes of glutamate receptors after the activation of A_1R could also interact with these results (Chen et al., 2015). The authors of this study analyzing the NMDA-based excitotoxicity used an inducible expression system that might be able to reveal acute effects of A_1R-dependent signaling, whereas our knockout model might be compromised by developmental effects. Similarly, the hyperexcitability of mitral cells was modified by a lack of A_1R expression. Finally, in our *in vivo* studies, we could not reveal an A_1R-dependent neuroprotective phenotype during neuroinflammation. Thus, the potential beneficial effect of A_1R-signaling in neurons is likely overruled and fails to protect olfactory neurons from hyperexcitability, calcium overload, and injury during neuroinflammation.

A possible explanation for the lack of neuroprotective function *via* A_1R activation could be the affinity of the P1 receptors to their ligand adenosine depending on the extracellular concentration. In contrast to the low-affinity receptors $A_{2B}R$ and A_3R, the A_1R and the $A_{2A}R$ show a high affinity to adenosine. While activation of A_1R is already present at low extracellular concentrations of adenosine (0.3–3 nM), which are mainly found under physiological conditions, activation of the $A_{2A}R$ requires a 10-fold rise of the extracellular adenosine concentration (Stockwell et al., 2017). According to these pharmacological properties, the inhibitory and neuroprotective capacity of A_1R could be overruled by the action of $A_{2A}R$ that acts as a counterpart. This could result in a dominance of $A_{2A}R$-mediated signaling in EAE. Another explanation could be the internalization of A_1R due to chronic activation (Klaasse et al., 2008). Several studies show that during chronic caffeine consumption, tolerance of A_1R to caffeine occurs by internalization. In parallel, the $A_{2A}R$ becomes predominant in the action of caffeine (Nehlig et al., 1992). In conclusion, the high level of extracellular adenosine during neuroinflammation could paradoxically lead to the suppression of neuroprotective adenosine-dependent downstream effects in neurons.

Moreover, the observations by Tsutsui et al. (2004) that the constitutive global A_1R knockout exacerbates EAE severity is in agreement with our results, as they attribute this effect to the immunosuppressive function of A_1R-signaling (Tsutsui et al., 2004). As A_1R is mainly expressed on immature dendritic cells, macrophages, and neutrophils in which its activity suppresses their activation, an A_1R deficiency would be expected to exacerbate CNS inflammatory disease (Cekic and Linden, 2016). The results obtained with the neuron-specific A1R knockout have some limitations. Combining the low throughput patch clamp-technique with the animal model of EAE revealed first insights into the olfactory bulb-specific response to inflammation. However, in some analyses Bayesian statistics, applied to evaluate negative results, revealed Bayes factors greater than 0.33. This indicates that we cannot entirely exclude that the absence of an effect is due to low statistical power. At this point, however, data of the global A_1R knockout and our data with the neuron-specific A_1R knockout suggest that neuronally expressed A_1R plays a minor role in resilience to inflammation in the EAE model.

MATERIALS AND METHODS

Mice

All mice [*C57Bl/6J* wild type (The Jackson Laboratory), $A_1R^{flx/flx}$ mice (provided by Frank Kirchhoff, Homburg, Germany) (Scammell et al., 2003), *SNAP25-IRES-Cre* mice (The Jackson Laboratory) (Harris et al., 2014), "*Tagger*" knockin mouse line provided by Walker Scot Jackson (Kaczmarczyk et al., 2019)] were kept under specific pathogen-free conditions in the central animal facility of the University Medical Center Hamburg-Eppendorf, Hamburg, Germany. Neuron-specific knockout mice with or without fluorescent nuclear tag ($A_1R^{flx/flx};SNAP25^{Cre}$, $A_1R^{flx/flx};Tag;SNAP25^{Cre}$) were generated by crossing $A_1R^{flx/flx}$ with *SNAP25-IRES-Cre* with or without the "*Tagger*" reporter mouse line (Kaczmarczyk et al., 2019). Mice were housed in a facility at 24 ± 2°C and 55–65% humidity with a 12-h light/dark cycle and had free access to food and water. Sex and age-matched adult animals (8–16 weeks of age) were used in all experiments. For behavioral experiments, animals were housed in an inverted light/dark cycle to enable the performance of the animal experiments in the animal's active day phase. Animals were adapted to the inverted light/dark cycle at least 3 weeks in advance. Experiments were carried out under red light and light exposure of less than 25 lux.

Mouse Tissue Preparation for Acute Slices

Olfactory bulbs were dissected, and horizontal brain slices were prepared as described before (Fischer et al., 2020). Briefly, olfactory bulbs were quickly transferred into a chilled slicing artificial cerebrospinal fluid (ACSF) that contained (in mM): NaCl, 83; $NaHCO_3$, 26.2; NaH_2PO_4, 1; KCl, 2.5; sucrose, 70; D-glucose, 20; $CaCl_2$, 0.5; $MgSO_4$, 2.5. About 200 μm thick acute slices of the bulbs were cut using a vibrating blade microtome (Leica VT1200S, Bensheim, Germany). The brain slices were stored in ACSF containing (in mM): NaCl, 120; $NaHCO_3$, 26; NaH_2PO_4, 1; KCl, 2.5; D-glucose, 2.8; $CaCl_2$, 2; $MgCl_2$, 1. Storage lasted for 30 min at 30°C and at least 30 min at RT before starting the experiments. The ACSF was continuously gassed with carbogen (95% of O_2 and 5% of CO_2; buffered to pH 7.4 with CO_2/bicarbonate).

Electrophysiological Recordings

Mitral cells of the main olfactory bulb were investigated using the patch clamp technique (EPC 10 amplifier, HEKA Elektronik GmbH Reutlingen, Germany). Throughout the experiments, the brain slices were superfused with ACSF. Drugs were applied with the perfusion system driven by a peristaltic pump (Reglo, Ismatec, Wertheim, Germany) at a flow rate of 2 ml min^{-1}. Application bars reflect the time window during which drug-containing ACSF is present in the bath. The whole

cell configuration was employed using patch pipettes with a resistance of ∼3–5 MΩ for mitral cells and ∼4–6 MΩ for granule cells. Recordings were digitized at 10–20 kHz and filtered (Bessel filter, 22 kHz). The standard pipette solution contained (in mM) the following: NaCl, 10; potassium gluconate, 105; K_{3-}-citrate, 20; Hepes, 10; $MgCl_2$, 0.5; Mg-ATP, 3; Na-GTP, 0.5; EGTA, 0.25. Cells were held at −50 mV in voltage clamp recordings and from −50 to −55 mV in current clamp recordings by appropriate current injection. High chloride pipette solution contained (in mM) the following: CsCl, 120; Hepes, 10; EGTA, 0.2; $MgCl_2$, 2; $CaCl_2$, 0.075; Na-ATP, 2; Na-GTP, 0.5; 4-AP, 5; TEA-Cl, 20. Cells were held at −70 mV in a voltage clamp recording with high chloride pipette solution. For mitral cell membrane property measurements, only cells of confirmed wildtype and knockout phenotype, that is, only cells that showed adenosine-induced outward current in wildtype and absence of adenosine-induced outward current in knockout animals, respectively, were included in the analysis. Series resistance (R_{series}) was monitored during the recording, and cells exceeding 20 MΩ and/or a change of 20% in R_{series} were excluded from the analysis. Cells exceeding an input resistance of 500 MΩ were also excluded from the analysis. Current clamp recordings for F/I plot were performed in the presence of 10 μM of NBQX, 50 μM of DAP-V, and 5 μM of gabazine. For the recording of current-voltage relationship in the voltage clamp, 0.5 μM of TTX was added, currents displayed are not leak subtracted, and voltages displayed are not corrected for liquid junction potential (−17 mV for potassium glutamate intracellular solution). For recordings of the adenosine effect in granule cells, series resistance was monitored and cells with R_{series} higher than 30 MΩ and/or a change of 20% during the recording were excluded from the analysis. Electrophysiological data were analyzed using *Mini Analysis* (Synaptosoft, Fort Lee, NJ, United States), *ClampFit* (Molecular Devices), *Review* (Bruxton), and *OriginPro* (Northampton, MA, United States).

Behavioral Tests

Mice were transferred from the breeding facility into a vivarium and maintained under standard housing with an inverted 12h/12h-light/dark cycle (light off at 8:00 am), i.e., experiments were transduced during the dark phase. All tests were performed with 10–16-week-old mice in a room next to the vivarium illuminated with dim red light. Tests started and ended at least 2 h after light offset and 3 h before light onset. The experimental material was cleaned with soap, water, and ethanol (70%) before and after each contact with an animal. All tests were video-recorded. Tracks representing the position of the mice were created and analyzed with the software, *EthoVision* (Noldus) as described (Freitag et al., 2003). Analysis of behavior with the software, *The Observer* (Noldus) was performed by a trained experimenter blind to the genotypes. The experimenter trained himself until he repeatedly scored at least 90% of consistency between two analyses performed at different times on the same mouse, as calculated with the Reliability Test provided by *The Observer* (having 1 s as maximal time discrepancy between two evaluations).

Olfactory Detection Test

Mice were examined in their ability to detect two new odors (vanilla and almond, Dr. Oetker) sequentially during a two-sided odor exposition in a test cage (Type II long, 325 mm × 170 mm × 140 mm) under red light. Mice were exposed in three trials of 4 min to either the empty tube (control) or a tube filled with a Whatman paper (0.6 cm Ø) containing 5 μl of the test odor of vanilla or almond. The tubes were placed at two openings in the middle of the short sides of the cage at a height of 3 cm from the bottom. The control tubes and test tubes were exchanged simultaneously on both sides of the cages to minimize a handling bias. Time sniffing at the tube was automatically measured by the video tracking system, *EthoVision* and offline manually by a trained experimenter blinded to experimental conditions using the software *The Observer*. Mice were habituated to the environment 5 days before the testing. This experiment was performed in healthy conditions with two cohorts with similar results. The EAE mice were tested at an early phase of EAE (severity score ≤1.5).

Trimethylthiazoline-Induced Freezing

A Whatman paper of 1 cm × 2 cm nourished with 10 μl of 15% of TMT was fixed to the side of a testcage (325 mm × 170 mm × 140 mm). Mice were placed in the test cage immediately. The cages were closed to avoid diffusion of the odor and exposition to other environmental stimuli. Reaction to the rising odor concentration was measured by the time of freezing in a trial of 12 min by a video tracking system (*EthoVision*) and manually by a rater, blinded to the genotype of the tested animal. Analyses were done under red light <20 lux. Mice were tested in a healthy condition or at an early phase of EAE (severity score ≤1.5).

Open Field

The open-field test was performed in a box (50 cm × 50 cm and 40 cm high) illuminated with white light (10 lux). Mice were placed in one corner of the box and their behavior was analyzed for 15 min. Distance moved, mean minimal distance to the wall, and time spent in the center (an imaginary 25 cm × 25 cm square in the middle of the arena) were analyzed with the *EthoVision* software. In contrast, the parameters rearing on the wall (mouse stands on hind limbs and touches the wall with at least one forepaw) and self-grooming were analyzed with *The Observer*.

Elevated Plus-Maze

The maze has the shape of a plus with four 30 cm long and 5 cm wide arms, connected by a squared center (5 cm × 5 cm). Two opposing arms are bordered by 15 cm high walls (closed arms), whereas 2 mm rim borders the other two arms (open arms). The maze was elevated 75 cm from the floor, and an infrared camera was allowed for video recording. The mouse was placed in the center facing one open arm and left in the maze for 5 min. The following parameters were analyzed with *The Observer*: entries into open and closed arms (calculated when all four paws were on an arm), total transitions (sum of entries into open and closed arms), entries into edges of open arms (calculated when the

mouse reaches with its snout the edge of an open arm), latency to enter into open arms, latency to reach the edge of an open arm, stretched attend posture toward the open arm, rearing, self-grooming, head dips from "protected" area (head movements over the side of an open arm with the snout pointing downward while the mouse remains in the center or closed arm), and head dips from "unprotected" area (head dips are done as the mouse is on the open arms).

Experimental Autoimmune Encephalomyelitis Induction and Scoring

For the induction of EAE, the mice were anesthetized with 1% of isoflurane to 2% v/v oxygen and immunized subcutaneously with 200 μg of myelin oligodendrocyte glycoprotein 35–55 (MOG_{35-55}) peptide (peptides elephants) in emulsion with complete Freund's adjuvant (BD) containing 4 mg ml^{-1} of *Mycobacterium tuberculosis* (BD). This is followed by the administration of 200 ng of PTX in PBS on the day of immunization and at day 2 after immunization. Animals were assessed daily. Clinical signs of EAE were scored as follows: 0, no clinical deficits; 1, tail weakness; 2, hind limb paresis; 3, partial hind limb paralysis; 3.5, full hind limb paralysis; 4, full hind limb paralysis, and forelimb paresis; 5, premorbid, or dead. Animals reaching a clinical score $\geq\geq$4 had to be killed according to the regulations of the Animal Welfare Act.

Mouse Tissue Preparation and Immunohistochemistry

Mice were anesthetized intraperitoneally with 100 μl of solution [10 mg ml^{-1} of esketamine hydrochloride (Pfizer), 1.6 mg ml^{-1} of xylazine hydrochloride (Bayer) dissolved in water] per 10 g of body weight. For histopathology and immunohistochemistry, the mice were perfused with 4% of paraformaldehyde (PFA), the brain tissue was dissected, fixed for 4 h with 4% of PFA, and then transferred to 30% of sucrose in PBS at 4°C. Main olfactory bulbs were sliced in 12 μm sections in coronal orientation with a freezing microtome (Leica Jung CM3000) and stored in a cryoprotective medium (Tissue Tek® from Sakura) at −80°C. Cryosections of olfactory bulb were incubated in 10% of normal donkey serum containing 0.1% of Triton X-100 and were subsequently stained with antibodies against the following: CNPase (mouse, Sigma-Aldrich; Cat# C5922, RRID: AB_476854), GFAP (chicken, Millipore; Cat# AB5541, RRID: AB_177521), HA-tag (rat, Sigma Aldrich; Cat# 11867423001, RRID: AB_390918), HuC/D (mouse, Molecular Probes; Cat# A-21271, RRID: AB_221448), Iba1 (rabbit, Wako Shibayagi; Cat# 019-19741, RRID: AB_839504), NeuN (chicken, Millipore; Cat# ABN91, RRID: AB_11205760), Reelin (mouse, Millipore; Cat# MAB5364, RRID: AB_2179313), and TH (mouse, Synaptic Systems; Cat# 213 104, RRID:AB_2619897). As secondary antibodies, we used Alexa Fluor 488–coupled donkey antibodies recognizing chicken IgG (1:600, Jackson Immunoresearch; Cat# 703-545-155, RRID: AB_2340375), rabbit IgG (1:600, Jackson Immunoresearch; Cat# 711-546-152, RRID: AB_2340619) and mouse IgG (1:600, Abcam; Cat# ab150105, RRID: AB_2732856), Alexa Fluor 647–coupled donkey antibodies recognizing rat IgG (1:600, Abcam; Abcam; Cat# ab150159, RRID: AB_2566823) and rabbit IgG (1:600, Abcam; Cat# ab150075, RRID: AB_2752244). To avoid background labeling when using anti-mouse primary antibodies in inflamed mouse tissue, we used a Fab fragment anti-mouse IgG (1:200, Jackson Immunoresearch, Cat# 715-007-003, RRID: AB_2307338) in 0.1% of Triton X-100 for 1 h before using the anti-mouse antibody. Images were acquired using a Zeiss LSM 700 confocal microscope. Samples were analyzed by the open-source package *Fiji* based on *ImageJ*. Reelin positive HuC/D positive and TH positive cells were counted manually restricted to the layer. The quantification of NeuN positive cells was automatized after binarization of the selected area using the threshold *triangle*.

Histopathology

For histopathology of EAE mice, the brain tissue was fixed with 4% PFA as mentioned above. After 4 h of fixation, the tissue was stored in PBS, cast in paraffin, and stained according to the standard procedures of the UKE Mouse Pathology Facility. For orientation in the tissue, hematoxylin staining (blue color) was done, followed by anti-CD3 primary antibodies (rabbit IgG, Abcam Cat# ab16669, RRID: AB_443425) and anti-Iba1 (rabbit IgG, Fujifilm Wako Shibayagi; Cat# 019-19741, RRID: AB_839504) that were visualized using the avidin–biotin complex technique with 3,3′-diaminobenzidine (brown stain). Slides were imaged with a *NanoZoomer 2.0-RS* digital slide scanner. CD3 positive and Iba1 positive cells were analyzed using the *NDP.view2* software (Hamamatsu) and the open-source software *Qpath*.[1]

Immunofluorescence

Olfactory bulb neurons (DIV 16–18) were fixed with 4% of PFA for 10 min at room temperature, permeabilized with 0.05% of Triton and blocked with 10% of normal donkey serum in PBS. Cells were incubated for 2 h with antibodies directed against A_1R (rabbit, Novus Biologicals; Cat# NB300-549, RRID: AB_10002337) and microtubule-associated protein 2 (MAP2, chicken, 1:2500; Abcam; Cat# ab5392, RRID: AB_2138153). As secondary antibodies, we used Alexa Fluor 488–coupled donkey antibodies recognizing chicken IgG (1:600, Jackson; Cat# 703-545-155, RRID: AB_2340375) and Alexa Fluor 647–coupled donkey antibodies recognizing rabbit IgG (1:600, Abcam; Cat# ab150075, RRID: AB_2752244). Images were taken with a Zeiss LSM 700 confocal microscope.

Primary Neuron Culture

Primary olfactory bulb cultures were prepared from E16.5 embryos. Olfactory bulb pieces were incubated in 0.05% of Trypsin-EDTA (Gibco) for 6 min at 37°C. Trypsination was stopped by DMEM-F12 containing 10% of FCS. Afterward, tissue was dissociated in HBSS and centrifuged for 2 min at 500 × *g*. The pellet was resuspended in primary growth medium (PGM), and cells were plated at 1×10^5 per cm^2 on poly-d-lysine-coated cell culture plates. We maintained cells in Primary Neuron Growth Medium BulletKit (PNGM, Lonza) at 37°C, 5% of CO_2, and relative humidity of 98%. To inhibit glial proliferation, we added

[1] https://qupath.github.io/

cytarabine (Sigma, 1 μM = AraC) and maintained cultures for 14–18 days *in vitro*.

Cell Viability Assay

Olfactory bulb primary neuron cultures were seeded in 96-well cell culture plates (Greiner, 655094) coated with poly-d-lysine as described above. Cell viability was measured by non-lytic NanoLuc Luciferase reaction assay (Promega, RealTime-Glo™ MT cell viability assay, G9711) in a plate reader (Tecan Spark Cyto) over 24 h. Treatment was added 5 h after the substrate and enzyme of RealtimeGlo™ to stabilize the luciferase reaction.

Quantitative Real-Time PCR

Isolated RNA was reversed transcribed to cDNA with the RevertAid H Minus First Strand cDNA Synthesis Kit (Thermo Fisher Scientific) according to the manufacturer's instructions. Gene expression was analyzed by real-time PCR performed in an ABI Prism 7900 HT Fast Real-Time PCR System (Applied Biosystems) using TaqMan Gene Expression Assays (Thermo Fisher Scientific) for *Adora1* (Mm01308023_m1), *Adora2* (Mm00802075_m1) and *Tbp* (Mm00446971_m1), and *Cdhr1* (Mm00499982_m1) and *Tbp* (Mm01277042_m1). Gene expression was calculated as $2^{-\Delta Ct}$ relative to *Tbp* as the endogenous control.

Statistics

Experimental data were analyzed within the R environment using *Rstudio* (version 1.2.5033) and *GraphPad Prism* (version 9.3.1). The data are presented as mean ± SEM throughout, and differences between two experimental groups were determined using unpaired, two-tailed Student's *t*-tests, and were FDR corrected for multiple comparisons or Mann–Whitney *U*-test according to normality distribution test by Shapiro–Wilk. Statistical analysis of the clinical scores in the EAE experiments was performed by applying the Mann–Whitney *U*-test to the AUCs for each animal. Repeated and paired measurements (trial and odor in the olfactory detection test, and time bins in the open field and TMT-induced freezing test) were analyzed by mixed two- or three-way ANOVA with genotype as a between-groups factor and the appropriate within-groups factor(s) followed by Dunnet's *post-hoc* analysis when appropriate. Electrophysiological data are indicated as mean ± SEM and were analyzed by ORIGINPro software using Mann–Whitney and Wilcoxon ranking tests for unpaired samples and paired samples, respectively. Validity of negative results obtained in frequentist statistical approaches were tested by Bayesian statistics using JASP software (Keysers et al., 2020). Resulting Bayes factors (BF_{10}) indicate the following on a linear scale: $BF_{10} < 0.3$ is the evidence of absence of an effect (samples are equal); $0.3 < BF_{10} < 3$ is the absence of evidence (no final conclusion permissible); $BF_{10} > 3$ is the evidence of effect (samples are different). The exact number of experiments is provided in the figure legends. All tests were two-tailed, and significances are indicated by $P < 0.05$, $P < 0.01$, and $P < 0.001$.

DATA AVAILABILITY STATEMENT

The original contributions presented in this study are included in the article/**Supplementary Material**, further inquiries can be directed to the corresponding authors.

ETHICS STATEMENT

All animal care and experimental procedures were performed according to institutional guidelines and conformed to requirements of the German Animal Welfare Act. All animal experiments were approved by the local ethics committee (Behörde für Soziales, Familie, Gesundheit und Verbraucherschutz in Hamburg: 122/17). We conducted all procedures in accordance with the ARRIVE guidelines (Kilkenny et al., 2010).

AUTHOR CONTRIBUTIONS

CS, DH, FM, and MF designed the experiments for the study and wrote the manuscript. CS, DH, KS, AO, A-LP, and FM analyzed the data. CS, KS, ST, DH, FM, A-LP, and SR performed experiments. All authors contributed to the article and approved the submitted version.

FUNDING

This work was supported by the Deutsche Forschungsgemeinschaft SFB1328 project A16 (DH and MF).

ACKNOWLEDGMENTS

We thank the members of the SFB1328 for the inspiring and lively discussions about the mechanisms of adenine nucleotide signaling. We would like to thank the members of the Friese laboratory for discussions and critical reading of the manuscript. We would also like to thank the UKE Mouse Pathology Facility for immunohistochemistry and Larissa Milde for providing preliminary data.

SUPPLEMENTARY MATERIAL

The Supplementary Material for this article can be found online at: https://www.frontiersin.org/articles/10.3389/fncel.2022.912030/full#supplementary-material

REFERENCES

Abraham, N. M., Egger, V., Shimshek, D. R., Renden, R., Fukunaga, I., Sprengel, R., et al. (2010). Synaptic inhibition in the olfactory bulb accelerates odor discrimination in mice. *Neuron* 65, 399–411. doi: 10.1016/J.NEURON.2010.01.009

Attfield, K. E., Jensen, L. T., Kaufmann, M., Friese, M. A., and Fugger, L. (2022). The immunology of multiple sclerosis.

Nat. Rev. Immunol. 28, 29–45. doi: 10.1038/S41577-022-00718-Z

Ballesteros-Yáñez, I., Castillo, C. A., Merighi, S., and Gessi, S. (2018). The role of adenosine receptors in psychostimulant addiction. *Front. Pharmacol.* 8:985. doi: 10.3389/fphar.2017.00985

Balu, R., Pressler, R. T., and Strowbridge, B. W. (2007). Multiple modes of synaptic excitation of olfactory bulb granule cells. *J. Neurosci.* 27:5621. doi: 10.1523/JNEUROSCI.4630-06.2007

Banie, A. P., and Nicholls, D. G. (1993). Adenosine A1 receptor inhibition of glutamate exocytosis and protein kinase c-mediated decoupling. *J. Neurochem.* 60, 1081–1086. doi: 10.1111/j.1471-4159.1993.tb03257.x

Biber, K., Klotz, K. N., Berger, M., Gebicke-Härter, P. J., and Van Calker, D. (1997). Adenosine A1 receptor-mediated activation of phospholipase C in cultured astrocytes depends on the level of receptor expression. *J. Neurosci.* 17, 4956–4964. doi: 10.1523/jneurosci.17-13-04956.1997

Boscia, F., Elkjaer, M. L., Illes, Z., and Kukley, M. (2021). Altered expression of ion channels in white matter lesions of progressive multiple sclerosis: what do we know about their function? *Front. Cell. Neurosci.* 15:214. doi: 10.3389/FNCEL.2021.685703/BIBTEX

Boyd, A. M., Sturgill, J. F., Poo, C., and Isaacson, J. S. (2012). Cortical feedback control of olfactory bulb circuits. *Neuron* 76, 1161–1174. doi: 10.1016/J.NEURON.2012.10.020

Bsteh, G., Hegen, H., Ladstätter, F., Berek, K., Amprosi, M., Wurth, S., et al. (2019). Change of olfactory function as a marker of inflammatory activity and disability progression in MS. *Mult. Scler.* 25, 267–274. doi: 10.1177/1352458517745724

Burnstock, G., Krügel, U., Abbracchio, M. P., and Illes, P. (2011). Purinergic signalling: from normal behaviour to pathological brain function. *Prog. Neurobiol.* 95, 229–274. doi: 10.1016/J.PNEUROBIO.2011.08.006

Burton, S. D. (2017). Inhibitory circuits of the mammalian main olfactory bulb. *J. Neurophysiol.* 118, 2034–2051. doi: 10.1152/JN.00109.2017

Carleton, A., Petreanu, L. T., Lansford, R., Alvarez-Buylla, A., and Lledo, P. M. (2003). Becoming a new neuron in the adult olfactory bulb. *Nat. Neurosci.* 6, 507–518. doi: 10.1038/nn1048

Carlin, J. L., Jain, S., Duroux, R., Suresh, R. R., Xiao, C., Auchampach, J. A., et al. (2018). Activation of adenosine A 2A or A 2B receptors causes hypothermia in mice. *Neuropharmacology* 139, 268–278. doi: 10.1016/J.NEUROPHARM.2018.02.035

Carruthers, A. M., Sellers, L. A., Jenkins, D. W., Jarvie, E. M., Feniuk, W., and Humphrey, P. P. A. (2001). Adenosine A1 receptor-mediated inhibition of protein kinase A-induced calcitonin gene-related peptide release from rat trigeminal neurons. *Mol. Pharmacol.* 59, 1533–1541. doi: 10.1124/mol.59.6.1533

Cauwels, A., Rogge, E., Vandendriessche, B., Shiva, S., and Brouckaert, P. (2014). Extracellular ATP drives systemic inflammation, tissue damage and mortality. *Cell Death Dis.* 53, e1102–e1102. doi: 10.1038/cddis.2014.70

Cekic, C., and Linden, J. (2016). Purinergic regulation of the immune system. *Nat. Rev. Immunol.* 16, 177–192. doi: 10.1038/nri.2016.4

Chasse, R., Malyshev, A., Fitch, R. H., and Volgushev, M. (2021). Altered heterosynaptic plasticity impairs visual discrimination learning in adenosine A1 receptor knockout mice. *J. Neurosci.* 41, 4631–4640. doi: 10.1523/jneurosci.3073-20.2021

Chen, J. F., Xu, K., Petzer, J. P., Staal, R., Xu, Y. H., Beilstein, M., et al. (2001). Neuroprotection by caffeine and A(2A) adenosine receptor inactivation in a model of Parkinson's disease. *J. Neurosci.* 21:RC143. doi: 10.1523/JNEUROSCI.21-10-J0001.2001

Chen, Z., Stockwell, J., and Cayabyab, F. S. (2015). Adenosine A1 receptor-mediated endocytosis of ampa receptors contributes to impairments in long-term potentiation (LTP) in the middle-aged rat hippocampus. *Neurochem. Res.* 41, 1085–1097. doi: 10.1007/S11064-015-1799-3

Coppi, E., Dettori, I., Cherchi, F., Bulli, I., Venturini, M., Pedata, F., et al. (2021). New insight into the role of adenosine in demyelination, stroke and neuropathic pain. *Front. Pharmacol.* 11:2403. doi: 10.3389/FPHAR.2020.625662/BIBTEX

Corradetti, R., Lo Conte, G., Moroni, F., Beatrice Passani, M., and Pepeu, G. (1984). Adenosine decreases aspartate and glutamate release from rat hippocampal slices. *Eur. J. Pharmacol.* 104, 19–26. doi: 10.1016/0014-2999(84)90364-9

Crespo, C., Liberia, T., Blasco-Ibáñez, J. M., Nácher, J., and Varea, E. (2013). The circuits of the olfactory bulb. the exception as a rule. *Anat. Rec.* 296, 1401–1412. doi: 10.1002/AR.22732

Cunha, R. A. (2016). How does adenosine control neuronal dysfunction and neurodegeneration? *J. Neurochem.* 139, 1019–1055. doi: 10.1111/jnc.13724

de Mendonça, A., Sebastião, A. M., and Ribeiro, J. A. (1995). Inhibition of NMDA receptor-mediated currents in isolated rat hippocampal neurones by adenosine A1 receptor activation. *Neuroreport* 6, 1097–1100. doi: 10.1097/00001756-199505300-00006

Deaglio, S., and Robson, S. C. (2011). Ectonucleotidases as regulators of purinergic signaling in thrombosis, inflammation, and immunity. *Adv. Pharmacol.* 61:301. doi: 10.1016/B978-0-12-385526-8.00010-2

Di Virgilio, F., Sarti, A. C., and Coutinho-Silva, R. (2020). Purinergic signaling, DAMPs, and inflammation. *Am. J. Physiol. - Cell Physiol.* 318, C832–C835. doi: 10.1152/ajpcell.00053.2020

Dickenson, J. M., Blank, J. L., and Hill, S. J. (1998). Human adenosine A1 receptor and P2Y2-purinoceptor-mediated activation of the mitogen-activated protein kinase cascade in transfected CHO cells. *Br. J. Pharmacol.* 124, 1491–1499. doi: 10.1038/sj.bjp.0701977

Dunwiddie, T. V., Basile, A. S., and Palmer, M. R. (1984). Electrophysiological responses to adenosine analogs in rat hippocampus and cerebellum: evidence for mediation by adenosine receptors of the A1 subtype. *Life Sci.* 34, 37–47. doi: 10.1016/0024-3205(84)90328-X

Dunwiddie, T. V., Diao, L., and Proctor, W. R. (1997). Adenine nucleotides undergo rapid, quantitative conversion to adenosine in the extracellular space in rat hippocampus. *J. Neurosci.* 17, 7673–7682. doi: 10.1523/JNEUROSCI.17-20-07673.1997

Egger, V., and Kuner, T. (2021). Olfactory bulb granule cells: specialized to link coactive glomerular columns for percept generation and discrimination of odors. *Cell Tissue Res.* 383, 495–506. doi: 10.1007/s00441-020-03402-7

Egger, V., and Urban, N. N. (2006). Dynamic connectivity in the mitral cell-granule cell microcircuit. *Semin. Cell Dev. Biol.* 17, 424–432. doi: 10.1016/J.SEMCDB.2006.04.006

Fenton, R. A., Shea, L. G., Doddi, C., and Dobson, J. G. (2010). Myocardial adenosine A1-receptor-mediated adenoprotection involves phospholipase C, PKC-ε, and p38 MAPK, but not HSP27. *Am. J. Physiol. - Hear. Circ. Physiol.* 298:H1671. doi: 10.1152/AJPHEART.01028.2009

Fischer, T., Scheffler, P., and Lohr, C. (2020). Dopamine-induced calcium signaling in olfactory bulb astrocytes. *Sci. Rep.* 10, 1–11. doi: 10.1038/s41598-020-57462-4

Fredholm, B. B. (2014). Adenosine - A physiological or pathophysiological agent? *J. Mol. Med.* 92, 201–206. doi: 10.1007/s00109-013-1101-6

Fredholm, B. B., IJzerman, A. P., Jacobson, K. A., Linden, J., and Müller, C. E. (2011). International union of basic and clinical pharmacology. LXXXI. Nomenclature and classification of adenosine receptors - an update. *Pharmacol. Rev.* 63, 1–34. doi: 10.1124/pr.110.003285

Fredholm, B. B., Irenius, E., Kull, B., and Schulte, G. (2001). Comparison of the potency of adenosine as an agonist at human adenosine receptors expressed in Chinese hamster ovary cells. *Biochem. Pharmacol.* 61, 443–448. doi: 10.1016/S0006-2952(00)00570-0

Freitag, S., Schachner, M., and Morellini, F. (2003). Behavioral alterations in mice deficient for the extracellular matrix glycoprotein tenascin-R. *Behav. Brain Res.* 145, 189–207. doi: 10.1016/S0166-4328(03)00109-8

Friese, M. A., Schattling, B., and Fugger, L. (2014). Mechanisms of neurodegeneration and axonal dysfunction in multiple sclerosis. *Nat. Rev. Neurol.* 10, 225–238. doi: 10.1038/nrneurol.2014.37

Futatsuki, T., Yamashita, A., Ikbar, K. N., Yamanaka, A., Arita, K., Kakihana, Y., et al. (2018). Involvement of orexin neurons in fasting- and central adenosine-induced hypothermia. *Sci. Rep.* 8:2717. doi: 10.1038/S41598-018-21252-W

Geramita, M. A., Burton, S. D., and Urban, N. N. (2016). Distinct lateral inhibitory circuits drive parallel processing of sensory information in the mammalian olfactory bulb. *Elife* 5:e16039. doi: 10.7554/ELIFE.16039

Giménez-Llort, L., Fernández-Teruel, A., Escorihuela, R. M., Fredholm, B. B., Tobeña, A., Pekny, M., et al. (2002). Mice lacking the adenosine A1 receptor are anxious and aggressive, but are normal learners with reduced muscle strength and survival rate. *Eur. J. Neurosci.* 16, 547–550. doi: 10.1046/j.1460-9568.2002.02122.x

Gnad, T., Navarro, G., Lahesmaa, M., Reverte-Salisa, L., Copperi, F., Cordomi, A., et al. (2020). Adenosine/A2B receptor signaling ameliorates the effects of aging and counteracts obesity. *Cell Metab.* 32, 56.e–70.e. doi: 10.1016/J.CMET.2020.06.006

Goektas, O., Schmidt, F., Bohner, G., Erb, K., Lüdemann, L., Dahlslett, B., et al. (2011). Olfactory bulb volume and olfactory function in patients with multiple sclerosis. *Rhinology* 49, 221–226. doi: 10.4193/Rhino10.136

Gomes, C. V., Kaster, M. P., Tomé, A. R., Agostinho, P. M., and Cunha, R. A. (2011). Adenosine receptors and brain diseases: neuroprotection and neurodegeneration. *Biochim. Biophys. Acta - Biomembr.* 1808, 1380–1399. doi: 10.1016/J.BBAMEM.2010.12.001

Gomez-Castro, F., Zappettini, S., Pressey, J. C., Silva, C. G., Russeau, M., Gervasi, N., et al. (2021). Convergence of adenosine and GABA signaling for synapse stabilization during development. *Science* 374:eabk2055. doi: 10.1126/SCIENCE.ABK2055

Gourine, A. V., Wood, J. D., and Burnstock, G. (2009). Purinergic signalling in autonomic control. *Trends Neurosci.* 32, 241–248. doi: 10.1016/j.tins.2009.03.002

Gundlfinger, A., Bischofberger, J., Johenning, F. W., Torvinen, M., Schmitz, D., and Breustedt, J. (2007). Adenosine modulates transmission at the hippocampal mossy fibre synapse via direct inhibition of presynaptic calcium channels. *J. Physiol.* 582:263. doi: 10.1113/JPHYSIOL.2007.132613

Harris, J. A., Hirokawa, K. E., Sorensen, S. A., Gu, H., Mills, M., Ng, L. L., et al. (2014). Anatomical characterization of Cre driver mice for neural circuit mapping and manipulation. *Front. Neural Circuits* 8:76. doi: 10.3389/FNCIR.2014.00076

Healy, L. M., Stratton, J. A., Kuhlmann, T., and Antel, J. (2022). The role of glial cells in multiple sclerosis disease progression. *Nat. Rev. Neurol.* 18, 237–248. doi: 10.1038/s41582-022-00624-x

Isaacson, J. S. (2010). Odor representations in mammalian cortical circuits. *Curr. Opin. Neurobiol.* 20, 328–331. doi: 10.1016/J.CONB.2010.02.004

Isaacson, J. S., and Strowbridge, B. W. (1998). Olfactory reciprocal synapses: dendritic signaling in the CNS. *Neuron* 20, 749–761. doi: 10.1016/S0896-6273(00)81013-2

Islam, S., Ueda, M., Nishida, E., Wang, M. X., Osawa, M., Lee, D., et al. (2018). Odor preference and olfactory memory are impaired in olfaxin-deficient mice. *Brain Res.* 1688, 81–90. doi: 10.1016/J.BRAINRES.2018.03.025

Jagannath, A., Varga, N., Dallmann, R., Rando, G., Gosselin, P., Ebrahimjee, F., et al. (2021). Adenosine integrates light and sleep signalling for the regulation of circadian timing in mice. *Nat. Commun.* 12, 1–11. doi: 10.1038/s41467-021-22179-z

Jeong, H. J., Jang, I. S., Nabekura, J., and Akaike, N. (2003). Adenosine A1 receptor-mediated presynaptic inhibition of GABAergic transmission in immature rat hippocampal CA1 neurons. *J. Neurophysiol.* 89, 1214–1222. doi: 10.1152/jn.00516.2002

Jesudasan, S. J. B., Gupta, S. J., Churchward, M. A., Todd, K. G., and Winship, I. R. (2021). Inflammatory cytokine profile and plasticity of brain and spinal microglia in response to atp and glutamate. *Front. Cell. Neurosci.* 15:634020. doi: 10.3389/fncel.2021.634020

Johansson, B., Halldner, L., Dunwiddie, T. V., Masino, S. A., Poelchen, W., Gimenez-Llort, L., et al. (2001). Hyperalgesia, anxiety, and decreased hypoxic neuroprotection in mice lacking the adenosine A1 receptor. *Proc. Natl. Acad. Sci. U.S.A* 98, 9407–9412. doi: 10.1073/pnas.161292398

Joseph, A., and De Luca, G. C. (2016). Back on the scent: the olfactory system in CNS demyelinating diseases. *J. Neurol. Neurosurg. Psychiatry* 87, 1146–1154. doi: 10.1136/jnnp-2015-312600

Kaczmarczyk, L., Bansal, V., Rajput, A., Rahman, R. U., Krzyzak, W., Degen, J., et al. (2019). Tagger-A Swiss army knife for multiomics to dissect cell type-specific mechanisms of gene expression in mice. *PLoS Biol.* 17:e3000374. doi: 10.1371/journal.pbio.3000374

Kato, H. K., Gillet, S. N., Peters, A. J., Isaacson, J. S., and Komiyama, T. (2013). Parvalbumin-expressing interneurons linearly control olfactory bulb output. *Neuron* 80, 1218–1231. doi: 10.1016/J.NEURON.2013.08.036

Kawamura, M., Ruskin, D. N., and Masino, S. A. (2019). Adenosine A1 receptor-mediated protection of mouse hippocampal synaptic transmission against oxygen and/or glucose deprivation: a comparative study. *J. Neurophysiol.* 122, 721–728. doi: 10.1152/jn.00813.2018

Keysers, C., Gazzola, V., and Wagenmakers, E. J. (2020). Using bayes factor hypothesis testing in neuroscience to establish evidence of absence. *Nat. Neurosci.* 23, 788–799. doi: 10.1038/S41593-020-0660-4

Kilkenny, C., Browne, W. J., Cuthill, I. C., Emerson, M., and Altman, D. G. (2010). Improving bioscience research reporting: the ARRIVE guidelines for reporting animal research. *J. Pharmacol. Pharmacother.* 1:94. doi: 10.4103/0976-500X.72351

Kim, C. S., and Johnston, D. (2015). A1 adenosine receptor-mediated GIRK channels contribute to the resting conductance of CA1 neurons in the dorsal hippocampus. *J. Neurophysiol.* 113, 2511–2523. doi: 10.1152/jn.00951.2014

Kirsch, G. E., Codina, J., Birnbaumer, L., and Brown, A. M. (1990). Coupling of ATP-sensitive K+ channels to A1 receptors by G proteins in rat ventricular myocytes. *Am. J. Physiol. - Hear. Circ. Physiol.* 259, H820–H826. doi: 10.1152/ajpheart.1990.259.3.h820

Klaasse, E. C., IJzerman, A. P., de Grip, W. J., and Beukers, M. W. (2008). Internalization and desensitization of adenosine receptors. *Purinergic Signal.* 4, 21–37. doi: 10.1007/s11302-007-9086-7

Kobayakawa, K., Kobayakawa, R., Matsumoto, H., Oka, Y., Imai, T., Ikawa, M., et al. (2007). Innate versus learned odour processing in the mouse olfactory bulb. *Nature* 450, 503–508. doi: 10.1038/nature06281

Lazarus, M., Oishi, Y., Bjorness, T. E., and Greene, R. W. (2019). Gating and the need for sleep: dissociable effects of adenosine a1and a2areceptors. *Front. Neurosci.* 13:740. doi: 10.3389/fnins.2019.00740

Lee, H. G., Wheeler, M. A., and Quintana, F. J. (2022). Function and therapeutic value of astrocytes in neurological diseases. *Nat. Rev. Drug Discov.* 21, 339–358. doi: 10.1038/S41573-022-00390-X

Lein, E. S., Hawrylycz, M. J., Ao, N., Ayres, M., Bensinger, A., Bernard, A., et al. (2006). Genome-wide atlas of gene expression in the adult mouse brain. *Nat.* 2006, 168–176. doi: 10.1038/nature05453

Li, A., Rao, X., Zhou, Y., and Restrepo, D. (2020). Complex neural representation of odour information in the olfactory bulb. *Acta Physiol.* 228:e13333. doi: 10.1111/APHA.13333

Linster, C., and Cleland, T. A. (2009). Glomerular microcircuits in the olfactory bulb. *Neural networks* 22:1169. doi: 10.1016/J.NEUNET.2009.07.013

Liu, H., and Xia, Y. (2015). Beneficial and detrimental role of adenosine signaling in diseases and therapy. *J. Appl. Physiol.* 119, 1173–1182. doi: 10.1152/japplphysiol.00350.2015

Liu, Z.-W., and Gao, X.-B. (2007). Adenosine inhibits activity of hypocretin/orexin neurons via A1 receptor in the lateral hypothalamus: a possible sleep-promoting effect. *J. Neurophysiol.* 97:837. doi: 10.1152/JN.00873.2006

Lucassen, E. B., Turel, A., Knehans, A., Huang, X., and Eslinger, P. (2016). Olfactory dysfunction in Multiple Sclerosis: a scoping review of the literature. *Mult. Scler. Relat. Disord.* 6, 1–9. doi: 10.1016/J.MSARD.2015.12.002

Lutterotti, A., Vedovello, M., Reindl, M., Ehling, R., Dipauli, F., Kuenz, B., et al. (2011). Olfactory threshold is impaired in early, active multiple sclerosis. *Mult. Scler.* 17, 964–969. doi: 10.1177/1352458511399798

Miyamichi, K., Shlomai-Fuchs, Y., Shu, M., Weissbourd, B. C., Luo, L., and Mizrahi, A. (2013). Dissecting local circuits: parvalbumin interneurons underlie broad feedback control of olfactory bulb output. *Neuron* 80, 1232–1245. doi: 10.1016/j.neuron.2013.08.027

Munshi, R., Pang, I. H., Sternweis, P. C., and Linden, J. (1991). A1 adenosine receptors of bovine brain couple to guanine nucleotide-binding proteins Gi1. Gi2, and Go. *J. Biol. Chem.* 266, 22285–22289. doi: 10.1016/S0021-9258(18)54567-1

Nazario, L. R., da Silva, R. S., and Bonan, C. D. (2017). Targeting adenosine signaling in Parkinson's disease: from pharmacological to non-pharmacological approaches. *Front. Neurosci.* 11:658. doi: 10.3389/fnins.2017.00658

Nehlig, A., Daval, J. L., and Debry, G. (1992). Caffeine and the central nervous system: mechanisms of action, biochemical, metabolic and psychostimulant effects. *Brain Res. Rev.* 17, 139–170. doi: 10.1016/0165-0173(92)90012-B

Neville, K. R., and Haberly, L. B. (2004). "Olfactory CortexIn," in *The Synaptic Organization of the Brain*, 5th Edn, ed. G. M. Shepherd (Oxford: Oxford University Press), 415–454. doi: 10.1093/ACPROF:OSO/9780195159561.003.0010

Nunes, D., and Kuner, T. (2015). Disinhibition of olfactory bulb granule cells accelerates odour discrimination in mice. *Nat. Commun.* 6, 1–13. doi: 10.1038/ncomms9950

Nunes, D., and Kuner, T. (2018). Axonal sodium channel NaV1.2 drives granule cell dendritic GABA release and rapid odor discrimination. *PLoS Biol.* 16:e2003816. doi: 10.1371/JOURNAL.PBIO.2003816

Nunez-Parra, A., Maurer, R. K., Krahe, K., Smith, R. S., and Araneda, R. C. (2013). Disruption of centrifugal inhibition to olfactory bulb granule cells impairs olfactory discrimination. *Proc. Natl. Acad. Sci. U.S.A* 110, 14777–14782. doi: 10.1073/PNAS.1310686110/-/DCSUPPLEMENTAL

Pereira-Figueiredo, D., Nascimento, A. A., Cunha-Rodrigues, M. C., Brito, R., and Calaza, K. C. (2021). Caffeine and its neuroprotective role in ischemic events: a mechanism dependent on adenosine receptors . *Cell. Mol. Neurobiol.* doi: 10.1007/s10571-021-01077-4

Pressler, R. T., and Strowbridge, B. W. (2006). Blanes cells mediate persistent feedforward inhibition onto granule cells in the olfactory bulb. *Neuron* 49, 889–904. doi: 10.1016/J.NEURON.2006.02.019

Rall, W., Shepherd, G. M., Reese, T. S., and Brightman, M. W. (1966). Dendrodendritic synaptic pathway for inhibition in the olfactory bulb. *Exp. Neurol.* 14, 44–56. doi: 10.1016/0014-4886(66)90023-9

Reppert, S. M., Weaver, D. R., Stehle, J. H., and Rivkees, S. A. (1991). Molecular cloning and characterization of a rat A1-adenosine receptor that is widely expressed in brain and spinal cord. *Mol. Endocrinol.* 5, 1037–1048. doi: 10.1210/MEND-5-8-1037

Rotermund, N., Schulz, K., Hirnet, D., and Lohr, C. (2019). Purinergic signaling in the vertebrate olfactory system. *Front. Cell. Neurosci.* 13:112. doi: 10.3389/fncel.2019.00112

Rotermund, N., Winandy, S., Fischer, T., Schulz, K., Fregin, T., Alstedt, N., et al. (2018). Adenosine A 1 receptor activates background potassium channels and modulates information processing in olfactory bulb mitral cells. *J. Physiol.* 596, 717–733. doi: 10.1113/JP275503

Saito, H., Nishizumi, H., Suzuki, S., Matsumoto, H., Ieki, N., Abe, T., et al. (2017). Immobility responses are induced by photoactivation of single glomerular species responsive to fox odour TMT. *Nat. Commun.* 8, 1–10. doi: 10.1038/ncomms16011

Sakano, H. (2020). Developmental regulation of olfactory circuit formation in mice. *Dev. Growth Differ.* 62, 199–213. doi: 10.1111/DGD.12657

Santiago, A. R., Madeira, M. H., Boia, R., Aires, I. D., Rodrigues-Neves, A. C., Santos, P. F., et al. (2020). Keep an eye on adenosine: its role in retinal inflammation. *Pharmacol. Ther.* 210:107513. doi: 10.1016/j.pharmthera.2020.107513

Scammell, T. E., Arrigoni, E., Thompson, M. A., Ronan, P. J., Saper, C. B., and Greene, R. W. (2003). Focal deletion of the adenosine A1 receptor in adult mice using an adeno-associated viral vector. *J. Neurosci.* 23, 5762–5770. doi: 10.1523/jneurosci.23-13-05762.2003

Schampel, A., and Kuerten, S. (2017). Danger: high voltage—the role of voltage-gated calcium channels in central nervous system pathology. *Cells* 6:43. doi: 10.3390/cells6040043

Schattling, B., Fazeli, W., Engeland, B., Liu, Y., Lerche, H., Isbrandt, D., et al. (2016). Activity of NaV1.2 promotes neurodegeneration in an animal model of multiple sclerosis. *JCI Insight* 1:e89810. doi: 10.1172/jci.insight.89810

Schetinger, M. R. C., Morsch, V. M., Bonan, C. D., and Wyse, A. T. S. (2007). NTPDase and 5'-nucleotidase activities in physiological and disease conditions: new perspectives for human health. *BioFactors* 31, 77–98. doi: 10.1002/BIOF.5520310205

Schmidt, F. A., Maas, M. B., Geran, R., Schmidt, C., Kunte, H., Ruprecht, K., et al. (2017). Olfactory dysfunction in patients with primary progressive MS. *Neurol. Neuroimmunol. NeuroInflam.* 4:e369. doi: 10.1212/NXI.0000000000000369

Schoppa, N. E. (2006). Synchronization of olfactory bulb mitral cells by precisely timed inhibitory inputs. *Neuron* 49, 271–283. doi: 10.1016/J.NEURON.2005.11.038

Schulz, K., Rotermund, N., Grzelka, K., Benz, J., Lohr, C., and Hirnet, D. (2018). Adenosine A1 receptor-mediated attenuation of reciprocal dendro-dendritic inhibition in the mouse olfactory bulb. *Front. Cell. Neurosci.* 11:435. doi: 10.3389/fncel.2017.00435

Sebastiao, A. M., Cunha, R. A., Cascalheira, J. F., and Ribeiro, J. A. (1999). Chapter 15 Adenine nucleotides as inhibitors of synaptic transmission: role of localised ectonucleotidases. *Prog. Brain Res.* 120, 183–192. doi: 10.1016/S0079-6123(08)63555-4

Serchov, T., Atas, H. C., Normann, C., Van Calker, D., and Biber, K. (2012). Genetically controlled upregulation of adenosine A1 receptor expression enhances the survival of primary cortical neurons. *Mol. Neurobiol.* 46, 535–544. doi: 10.1007/s12035-012-8321-6

Sickmann, T., and Alzheimer, C. (2003). Short-term desensitization of G-protein-activated, inwardly rectifying K+ (GIRK) currents in pyramidal neurons of rat neocortex. *J. Neurophysiol.* 90, 2494–2503. doi: 10.1152/JN.00112.2003

Stockwell, J., Jakova, E., and Cayabyab, F. S. (2017). Adenosine A1 and A2A receptors in the brain: current research and their role in neurodegeneration. *Molecules* 22:676. doi: 10.3390/molecules22040676

Todd Pressler, R., and Strowbridge, B. W. (2020). Activation of granule cell interneurons by two divergent local circuit pathways in the rat olfactory bulb. *J. Neurosci.* 40, 9701–9714. doi: 10.1523/JNEUROSCI.0989-20.2020

Trussell, L. O., and Jackson, M. B. (1985). Adenosine-activated potassium conductance in cultured striatal neurons. *Proc. Natl. Acad. Sci. U. S. A* 82, 4857–4861. doi: 10.1073/pnas.82.14.4857

Tsutsui, S., Schnermann, J., Noorbakhsh, F., Henry, S., Yong, V. W., Winston, B. W., et al. (2004). A1 adenosine receptor upregulation and activation attenuates neuroinflammation and demyelination in a model of multiple sclerosis. *J. Neurosci.* 24, 1521–1529. doi: 10.1523/JNEUROSCI.4271-03.2004

Uecker, F. C., Olze, H., Kunte, H., Gerz, C., Göktas, O., Harms, L., et al. (2017). Longitudinal testing of olfactory and gustatory function in patients with multiple sclerosis. *PLoS One* 12:e0170492. doi: 10.1371/JOURNAL.PONE.0170492

Umemiya, M., and Berger, A. J. (1994). Activation of adenosine A1 and A2 receptors differentially modulates calcium channels and glycinergic synaptic transmission in rat brainstem. *Neuron* 13, 1439–1446. doi: 10.1016/0896-6273(94)90429-4

Wachowiak, M., and Shipley, M. T. (2006). Coding and synaptic processing of sensory information in the glomerular layer of the olfactory bulb. *Semin. Cell Dev. Biol.* 17, 411–423. doi: 10.1016/J.SEMCDB.2006.04.007

Woo, M. S., Ufer, F., Rothammer, N., Di Liberto, G., Binkle, L., Haferkamp, U., et al. (2021). Neuronal metabotropic glutamate receptor 8 protects against neurodegeneration in CNS inflammation. *J. Exp. Med.* 218:e20201290. doi: 10.1084/JEM.20201290/211853

Yang, L., Li, L. M., Yang, L. N., Zhang, L. J., Fu, Y., Li, T., et al. (2016). Olfactory dysfunction in patients with multiple sclerosis. *J. Neurol. Sci.* 365, 34–39. doi: 10.1016/j.jns.2016.03.045

Yang, M., and Crawley, J. N. (2009). Simple behavioral assessment of mouse olfaction. *Curr. Protoc. Neurosci.* 8:24. doi: 10.1002/0471142301.NS0824S48

Zhu, Y., and Ikeda, S. R. (1993). Adenosine modulates voltage-gated Ca2+ channels in adult rat sympathetic neurons. *J. Neurophysiol.* 70, 610–620. doi: 10.1152/jn.1993.70.2.610

Zimmermann, H. (2021). Ectonucleoside triphosphate diphosphohydrolases and ecto-5'-nucleotidase in purinergic signaling: how the field developed and where we are now. *Purinergic Signal.* 17, 117–125. doi: 10.1007/S11302-020-09755-6

Zitman, F. M. P., and Richter-Levin, G. (2013). Age and sex-dependent differences in activity, plasticity and response to stress in the dentate gyrus. *Neuroscience* 249, 21–30. doi: 10.1016/j.neuroscience.2013.05.030

Conflict of Interest: The authors declare that the research was conducted in the absence of any commercial or financial relationships that could be construed as a potential conflict of interest.

Publisher's Note: All claims expressed in this article are solely those of the authors and do not necessarily represent those of their affiliated organizations, or those of the publisher, the editors and the reviewers. Any product that may be evaluated in this article, or claim that may be made by its manufacturer, is not guaranteed or endorsed by the publisher.